ACS Photonics

Review

pubs.acs.org/journal/apchd5

Silicon–Organic and Plasmonic–Organic Hybrid Photonics

Wolfgang Heni,[†,⊥] Yasar Kutuvantavida,[‡,⊥] Christian Haffner,[†] Heiner Zwickel,[‡] Clemens Kieninger,[‡] Stefan Wolf,[‡] Matthias Lauermann,[‡] Yuriy Fedoryshyn,[†] Andreas F. Tillack,[§] Lewis E. Johnson,[§] Delwin L. Elder,[§] Bruce H. Robinson,[§] Wolfgang Freude,[‡] Christian Koos,[‡] Juerg Leuthold,[†] and Larry R. Dalton*[,§]

[†]Institute of Electromagnetic Fields, ETH Zurich, Zurich 8092, Switzerland

[‡]Institute of Photonics and Quantum Electronics (IPQ) and Institute of Microstructure Technology (IMT), Karlsruhe Institute of Technology (KIT), 76131 Karlsruhe, Germany

[§]Department of Chemistry, University of Washington, Seattle, Washington 98195-1700, United States

ABSTRACT: Chip-scale integration of electronics and photonics is recognized as important to the future of information technology, as is the exploitation of the best properties of electronics, photonics, and plasmonics to achieve this objective. However, significant challenges exist including matching the sizes of electronic and photonic circuits; achieving low-loss transition between electronics, photonics, and plasmonics; and developing and integrating new materials. This review focuses on a hybrid material approach illustrating the importance of both chemical and engineering concepts. Silicon–organic hybrid (SOH) and plasmonic–organic hybrid (POH) technologies have permitted dramatic improvements in electro-optic (EO) performance relevant to both digital and analog signal processing. For example, the voltage–length product of devices has been reduced to less than 40 Vμm, facilitating device footprints of <20 μm^2 operating with digital voltage levels to frequencies above 170 GHz. Energy efficiency has been improved to around a femtojoule/bit. This improvement has been realized through exploitation of field enhancements permitted by new device architectures and through theory-guided improvements in organic electro-optic (OEO) materials. Multiscale theory efforts have permitted quantitative simulation of the dependence of OEO activity on chromophore structure and associated intermolecular interactions. This has led to new classes of OEO materials, including materials of reduced dimensionality and neat (pure) chromophore materials that can be electrically poled. Theoretical simulations have helped elucidate the observed dependence of device performance on nanoscopic waveguide dimensions, reflecting the importance of material interfaces. The demonstration and explanation of the dependence of in-device electro-optic activity, voltage–length product, and optical insertion loss on device architecture (e.g., slot width) suggest new paradigms for further dramatic improvement of performance.

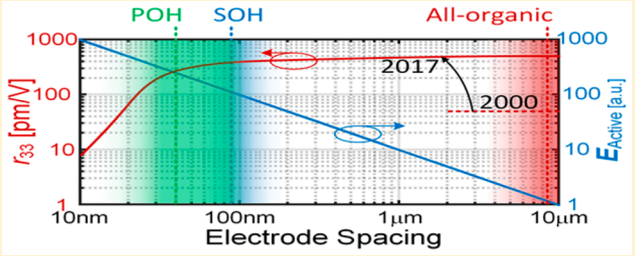

KEYWORDS: *organic electro-optic materials, chipscale electronic–photonic integration, high-speed optical interconnects, RF photonics, multiscale theoretical simulations, nanoscale device architectures, material interfaces, 2D materials*

Chip-scale photonic integration and chip-scale integration of electronics and photonics have long been recognized as critical next steps in the evolution of information technology. However, the substantial size mismatch between electronic and photonic circuits together with issues of energy efficiency, bandwidth, optical loss, drive voltage, and signal distortion related to active photonic devices have represented significant obstacles to the realization of chip-scale integration of electronics and photonics and to photonic integration in general. Another issue relates to the absence of photonic materials that make such integration obvious and straightforward, although it has been recognized that future integration will likely involve a combination of different materials (hybrid integration). There has also been an increasing interest in exploiting the best of electronics, photonics (including subwavelength photonics), and plasmonics (metal optics) to overcome the aforementioned obstacles. The advent of silicon photonics[1−22] has represented a hallmark event with respect to addressing the critical issues inhibiting photonic integration. Advances in plasmonics,[23−31] photonic crystal architectures,[32−45] and hybrid materials[46−92] have complemented the introduction of silicon photonics. Taken together, a transformative advance in information technology, comprising also telecommunications, computing, and sensing, is being realized. State-of-the-art technologies can be enhanced by the addition of high-performance organic electro-optic materials to form silicon–organic hybrid (SOH) and plasmonic–organic hybrid (POH) technologies,[46−89] although it is noted that a number of other hybrid device technologies exist[90−92] and are being aggressively pursued. Also, there has been an increasing interest in 2D materials such as graphene as a material for photonic

Received: March 8, 2017
Published: June 12, 2017

DOI: 10.1021/acsphotonics.7b00224
ACS Photonics 2017, 4, 1576–1590

integration applications.[93] As a caveat, it is noted that this communication does not suggest that any one technology is an obvious choice or that any one figure of merit can be universally applied to evaluate competitive advantage. Each potential application has different requirements for drive voltage, energy efficiency, optical loss, bandwidth, signal linearity, device footprint, cost, and operational lifetime, and thus different figures of merit and different technology choices will be relevant for different applications. However, we now focus on the impressive advances that have been made in many performance categories with respect to SOH and POH devices. For example, an important device figure of merit for electro-optic modulators, $U_\pi L$ (the π-voltage−length product), has been advanced from ≥10 Vcm for state-of-the-art lithium niobate modulators[94] to <500 Vμm for SOH devices[41,43−46,70] to <40 Vμm for POH modulators,[46,80] an improvement of more than 3 orders of magnitude. Reductions in $U_\pi L$ have translated into more compact devices; for example, devices with footprints of tens of square micrometers have been produced that operate at voltage levels that do not require electronic amplifiers. Moreover, energy efficiency has been improved to femtojoule/bit levels, bandwidths of greater than 170 GHz have been demonstrated, extinction ratios of greater than 25 dB have been realized, and optical insertion loss on the order of 5 dB has been achieved.[46,70,76,83] These performance parameters have led not only to record transmission rate demonstrations[76,83] in data communications and telecommunications but also to applications in the field of sensing and metrology.[78,83,84,89] Besides electro-optic modulators, polymer-based IR lasers have been demonstrated recently using the SOH integration concept.[95] These devices lend themselves to highly scalable light sources for low-cost biosensors.

This review focuses on advances that have been achieved recently with respect to SOH[46,66−70,73,76,77,79,81,87] and POH[46,62,71,72,74,75,78,80,82,84,85,88,89] electro-optic devices. These advances have required theory-guided advances in organic electro-optic (OEO) materials[96−109] together with exploitation of the advantages offered by new silicon photonic and plasmonic device architectures. The results of multiscale (correlated quantum and statistical mechanical) methods have shifted the focus from electrically poled polymer composite materials to high-number-density neat (pure) chromophore materials that yield electro-optic coefficients (r_{33}) upon poling of greater than 500 pm/V in thin films (compared to ∼32 pm/V for crystalline lithium niobate).[109−111] Moreover, theory has led the way to utilization of OEO materials with controlled lattice dimensionality (e.g., two-dimensional or Bessel lattice materials).[102] Treatment of complex soft matter OEO materials has required significant advances in multiple scale theoretical methods (e.g., coarse-grained Monte Carlo methods exploiting level-of-detail and adiabatic volume adjustment protocols[104,107,108]). These protocols are critical to achieve simulation methodologies capable of a quantitative prediction of in-device electro-optic activity and to understand complex issues such as the role of material interfaces. Silicon photonics, and in particular slotted silicon photonic waveguides as well as plasmonic waveguides, have facilitated confinement of both optical and radio frequency (dc to hundreds of GHz) fields into nanoscopic dimensions. Such confinement not only enhances optical field dependent nonlinearities but also dramatically increases electric field strengths (dc to terahertz (THz) frequencies), thereby contributing to a reduction of the $U_\pi L$ product in electro-optic modulators. New device architectures have required advances in both material processing/device fabrication protocols and device architecture concepts. Recently, it has been demonstrated that in-device electro-optic activity depends on waveguide geometry, such as the slot width, reflecting the importance of interfaces (e.g., between electrodes and the OEO material).[86] This realization has been broadened to understand the dependence of $U_\pi L$, r_{33}, and optical insertion loss on waveguide width, thus making waveguide architecture an even more important consideration in the design of electro-optic materials and devices.[86] In summary, the design paradigms for both materials and devices have changed dramatically over the past several years, and this review summarizes and discusses the importance of these changes.

EVOLUTION OF MATERIAL DESIGN OF ORGANIC CHROMOPHORES

Organic electro-optic materials hold the potential for permitting terahertz device bandwidths by exploiting the femtosecond (<30 fs) response times of the conjugated π-electron systems of organic chromophores to time-varying electric fields.[109] OEO materials also hold the potential for very large electro-optic activity due to the substantial charge redistribution that is induced by electric fields in long (nanometer length) conjugated systems; for example, values greater than 1000 pm/V could be achieved if dipolar chromophores are aligned in perfect acentric order.[109] Finally, OEO materials afford versatile and excellent processability, and when chromophores are prepared in kilogram quantities, OEO materials become very cost-effective.

Unfortunately, increasing the electro-optic activity of OEO materials has proven extremely difficult.[109] This review illustrates through consideration of theory-guided design why progress has been slow in the past but has recently accelerated. This review also points out problems associated with traditionally used equations including the equation relating electro-optic activity (r_{33}) to molecular properties, namely, $r_{33} = 2\beta(\omega, \epsilon)\rho_N\langle\cos^3\theta\rangle g(\omega, n)$, where $\beta(\omega, \epsilon)$ is the molecular first hyperpolarizability that is dependent on optical frequency ω and material dielectric permittivity ϵ; ρ_N is the chromophore number density, $\langle\cos^3\theta\rangle$ is the acentric order parameter, and $g(\omega, n)$ is the modified Lorentz−Onsager factor taking into account the dielectric properties of the environment surrounding the chromophores.[109] The second equation, which requires more detailed consideration, relates the π-voltage(U_π)−length-(L) parameter of devices to electro-optic activity, namely, $U_\pi L = \lambda w/(n^3 r_{33}\Gamma)$, where λ is the vacuum wavelength of the optical carrier, w is the electrode spacing, n is the index of refraction, and Γ is the field interaction factor, which is a measure of how strongly the optical field interacts with the OEO material in the slot.[46,51] This expression for $U_\pi L$ is appropriate for SOH devices;[51] however, for POH devices, which also benefit from the "slow-light effect", the equation becomes $U_\pi L = \lambda w/(n^2 r_{33}\Gamma_E n_{slow})$, where Γ_E denotes the field energy interaction factor and n_{slow} reflects the effect of reduced energy velocity in plasmonic slot waveguides.[72] These equations emphasize the dependence of $U_\pi L$ on device architecture. The equations for r_{33} and $U_\pi L$ are based on the assumption that the quantities on the right-hand sides of the equation are independent of each other and of waveguide dimensions. This is not the case for the best performing materials and devices. Indeed, detailed multiscale theoretical calculations are required to understand

DOI: 10.1021/acsphotonics.7b00224
ACS Photonics 2017, 4, 1576−1590

experimental results and guide the design of improved materials and devices.

To realize finite electro-optic activity with organic materials, there needs to be a net alignment of constituent dipolar chromophores with the applied radio frequency and optical fields.[109] In the case of introducing order by electric field poling, this corresponds to alignment in the direction of the poling field (which is also the direction of the applied radio frequency and optical electric fields). If the chromophores are perfectly aligned with the radio frequency and optical field electrical components, then $\langle\cos^3\theta\rangle = 1$. If chromophores are noninteracting and are free to rotate in three dimensions and if the thermal energy kT is approximately equal to the product of chromophore dipole moment and the poling field felt by the chromophores (μF), then $\langle\cos^3\theta\rangle \approx 0.2$. This is known as the Langevin limit and is very difficult to achieve because strong dipolar interactions among high-dipole-moment chromophores tend to favor centric order.[96−109] In the year 2000, organic materials used in electro-optic devices were almost exclusively chromophore−polymer composites[96−99,109] (although some studies involved crystalline materials and materials prepared by sequential synthesis methods[109]). Chromophore number densities leading to maximum electro-optic activity were approximately (2−3) × 10^{20} chromophores/cm^3, reflecting the fact that acentric order parameters ($\langle\cos^3\theta\rangle$) decreased with increasing chromophore number density as the result of increasing chromophore dipolar interactions and increased centrosymmetric pairing.[96−99] This resulted in a maximum being observed in the graph of r_{33} vs ρ_N. Theory demonstrated that electro-optic activity could be somewhat increased for a given poling field strength by making chromophores more spherical (decreasing the aspect ratio of the normally prolate-ellipsoid-shaped chromophores).[96−99] It was assumed that at high chromophore number densities poling-induced electro-optic activity would be zero. However, more recent theoretical simulations have shown that a second maximum (at higher ρ_N) is observed in the plot of electro-optic activity versus chromophore number density for high-dipole-moment chromophores (see Figure 1).[104,107,108]

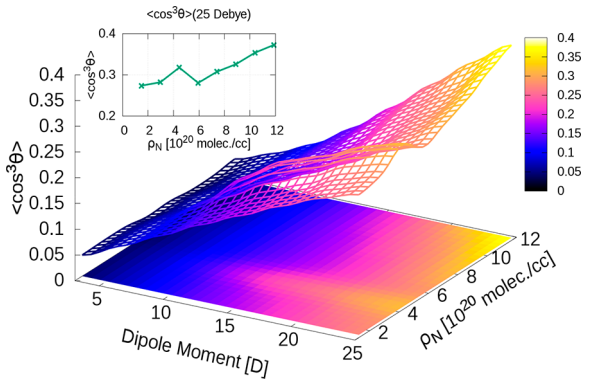

Figure 1. Simulation results (adiabatic volume adjustment method, followed by the NVT ensemble averaging, using a CLD-1-type molecule; see Figure 3 for the structure of CLD-1) are shown for a two-ellipsoid level-of-detail model for average acentric order, as functions of both chromophore dipole moment and number density. The surface mesh plot is color coded to represent the average acentric order, $\langle\cos^3\theta\rangle$ (given by the color bar). The inset shows the trace of average acentric order at the largest dipole moment, 25 D, corresponding to the experimentally expected dipole moment.

These theoretical predictions are consistent with experimental observations and have led to high chromophore number density materials (including neat materials) dominating current state-of-the-art OEO materials and utilization of such materials in devices. Neat high-dipole-moment chromophore materials have permitted larger electro-optic activity through improved chromophore number densities (e.g., >5 × 10^{20} chromophores/cm^3), emphasizing that it is the product $\rho_N\langle\cos^3\theta\rangle$ that must be optimized to optimize electro-optic activity. Some improvement is also realized through increased dielectric permittivity and the local field effect of higher chromophore number density materials. In addition, intermolecular electrostatic interactions among "designed" chromophores at high number densities can lead to reduced lattice dimensionality and thus improved electro-optic activity through the dependence of acentric order parameters on lattice dimensionality.[102,106,109] For a given poling field strength, maximum achievable acentric order increases as the dimensionality of the matrix surrounding a chromophore is decreased. Thus, theoretical simulations have supported the systematic design of new chromophores leading to state-of-the-art electro-optic activity (>500 pm/V in thin films).[109−111]

There are two important advances in coarse-grained Monte Carlo simulations that have led to efficient quantitative simulation of electro-optic activity for both low- and high-number-density electro-optic materials.[104,107,108] The level-of-detail (LoD) method uses variously shaped (e.g., ellipsoids) objects to efficiently model various segments (the conjugated π-electron core, phenyl rings, etc.) of complex chromophores at dramatically reduced computational cost relative to fully atomistic methods. For example, computational speed is increased by a factor of 1800 relative to fully atomistic calculations by representing the chromophore by a single prolate ellipsoid. The second component of the LoD method involves use of different levels of detail to model chromophores. For example, while a single ellipsoid is capable of modeling the chromophore core for low-number-density chromophore materials, multiple ellipsoids are necessary to model features such as chromophore curvature, which influences poling efficiency at high ρ_N (i.e., for close packing of chromophores). Representing a chromophore by two ellipsoids can account for chromophore curvature while still permitting an improvement of 610 in simulation time.

The adiabatic volume adjustment (AVA) method addresses the problem of chromophores being trapped in shallow local minima that prevent a true equilibrium distribution from being sampled within a reasonable number of configurations in conventional NVT simulations. AVA emulates the condensation of chromophores from solution (or gas phase); that is, the volume of the simulation space is reduced as the simulation process proceeds. Trapping of chromophores in local energetic minima (which favors centrosymmetric organization) leads to artificially reduced electro-optic activity. Simulations have thus provided insight not only into equilibrium chromophore organization but also into the dynamics of chromophore evolution under electric field poling and an explanation of why equilibrium distributions are sometimes not achieved for some materials.

Calculations of molecular first hyperpolarizabilities[102,105,109] employing well-tested quantum mechanical methods (hybrid density functional theory (DFT) and nth-order Møller−Plesset perturbation theory (MPn)) together with the aforementioned coarse-grained statistical mechanical simulations have led to

DOI: 10.1021/acsphotonics.7b00224
ACS Photonics 2017, 4, 1576−1590

quantitative prediction of electro-optic activity illustrating the sensitivity of electro-optic activity to subtle chromophore structural features, e.g., how $\rho_N\langle\cos^3\theta\rangle$ and $\langle\cos^3\theta\rangle$ change with chromophore modification (e.g., changing the size and shape of the bridge component). This is illustrated in Figure 2

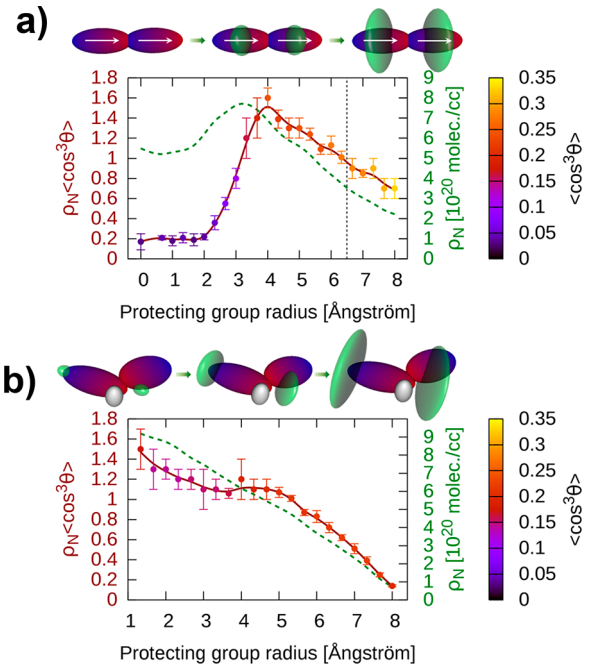

Figure 2. 3D simulations of properties related to OEO materials as a function of protecting group radius (green discs) for (a) a simplified, linear chromophore system with two dipoles at ellipsoid centers and (b) a CLD-1 (nonlinear or angled)-type chromophore system with charge distribution from DFT calculations. The filled circles represent the product of number density and acentric order, color coded by $\langle\cos^3\theta\rangle$. The dashed line indicates the equilibrium density (ρ_N) of the system. The dipole moment is 25 D.

for two hypothetical chromophore structures. The first is a linear chromophore, which is approximated by two ellipsoids with embedded dipoles. The second is a curved (bent) chromophore where the conformation and electron distribution have been derived from DFT calculations. For both basic structures, the variation of the product of number density and acentric order is shown as a function of increasing the size of protecting groups (green discs of the constituent ellipsoids). The experimental results for simple polyene bridge chromophores (see Figure 3) correspond to the plateau region of bent chromophore simulation. Theory suggests that modification of this type of chromophore by increasing the waist of the chromophore will lead to poorer electro-optic activity.

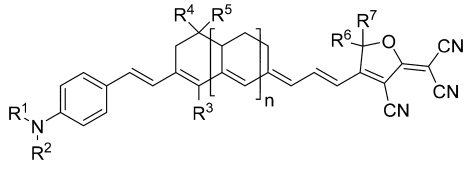

Figure 3. Generic structure of amine donor, isophorone-protected-polyene bridge, tricyanofuran acceptor chromophores discussed in this review. CLD-type chromophores correspond to n = 0, GLD-type chromophores correspond to n = 1, and ZLD-type chromophores correspond to n = 2.[109]

Theory also suggests that chromophore reorientation for this type of chromophore will be three-dimensional, although reduced dimensionality is expected for the linear chromophore at the highest number density. Modifying chromophores to include groups such as coumarin or arene/perfluoroarene (that exhibit long-range cooperative interactions) can reduce rotational freedom of chromophores under poling to approximately 2D, leading to enhanced poling efficiency and electro-optic activity.[102,109]

Figure 2 illustrates that modification of chromophores (e.g., to attenuate close approach of chromophores in unwanted orientations) can be carried too far. Modification decreases chromophore number density, and this can overwhelm modest increases achieved in acentric order. Figure 2 also illustrates that if linear chromophores could be produced, they would lead to improved acentric order and electro-optic activity. Clearly, not all structures suggested by theory can be synthesized, illustrating the importance of utilizing knowledge from quantum mechanics, statistical mechanics, and organic synthesis in a correlated manner.

Most recently, simulations of electro-optic activity (or more accurately, $\rho_N\langle\cos^3\theta\rangle$) in slotted waveguides as a function of slot width have been carried out.[86] The interaction between chromophores and electrodes at the interfaces results in a reduction in poling efficiency for the narrowest waveguides (see Figure 4).[86] Examination of the theoretical equilibrium

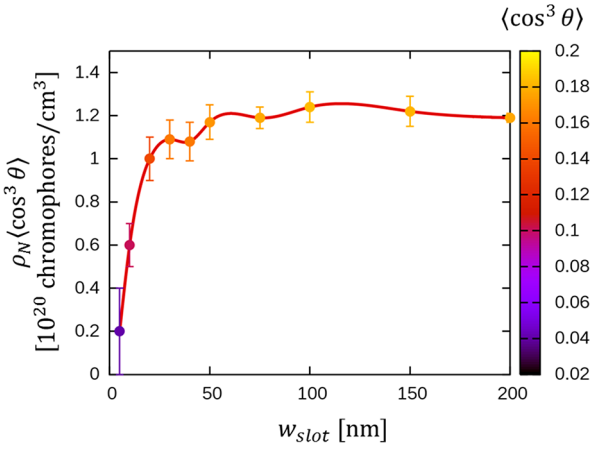

Figure 4. Simulated chromophore loading, $\rho_N\langle\cos^3\theta\rangle$, and acentric order, $\langle\cos^3\theta\rangle$, are shown as a function of the slot width for a plasmonic−organic hybrid device. The achieved average acentric order, $\langle\cos^3\theta\rangle$, is indicated by the color of the data points. Bulk-like acentric order is reached at slot widths of >100 nm. Adapted with permission from ref 86.

chromophore distributions shows that chromophores lie down along the electrode surfaces partially influenced by mirror charges and steric restrictions. This effect becomes more important as slot widths are reduced as the relative importance of interfaces relative to the bulk increases. Also, if vertical walls are slanted, acentric order can be attenuated; this effect can be evaluated by simulation. Of course, electrical characteristics of materials and features such as surface roughness also come into play and are also being treated. Theory also provides an avenue for systematically addressing these issues and even issues of electrical conductivity (charge transfer across interfaces).

For example, electrode surface modification (to overcome mirror charges and conductance) and/or sequential synthesis

DOI: 10.1021/acsphotonics.7b00224
ACS Photonics 2017, 4, 1576−1590

methods[109] employing covalent coupling of chromophores to each other and at interfaces (to overcome interactions that make chromophores want to lie down on the electrode surfaces) may permit dramatic improvement of acentric order for chromophores incorporated into slotted waveguide architectures with slot widths of less than 100 nm.[86]

New theoretical and experimental results have motivated the re-examination of previously pursued research directions. For example, two decades ago, sequential synthesis-self-assembly methods were pursued by a number of investigators.[109] At that time, electrode separations were on the order of 5−10 μm, requiring a thousand or more sequential synthetic steps. Thousands of synthetic steps are challenging even for automated processes. Moreover, defects tend to propagate, leading to reduced electro-optic activity and increased optical loss as the stepwise process proceeds. However, with electrode separations less than 100 nm, the number of steps is dramatically reduced, motivating reconsideration of the feasibility of this approach.

In like manner, chromophores with longer polyene bridges were synthesized in the late 1990s but were not pursued for device applications because device lengths at that time were 1−3 cm, and thus the optical propagation loss associated with such chromophores made an unacceptably high contribution to device insertion loss. However, for device lengths less than 1 mm, the propagation loss associated with such chromophores makes an insignificant contribution to device insertion loss. Thus, GLD and ZLD chromophores (see Figure 3) can now be utilized without significant increase in optical loss.[109,122] Both theoretical simulations and preliminary experimental results suggest that this is a productive route to improving electro-optic activity. The above two examples illustrate the importance of considering device architecture in development of new electro-optic materials and processing conditions.

Figure 3 illustrates that chromophores can be modified in a very large number of ways, and multiscale theoretical simulations are required to understand the impact of each modification on ultimate material performance. Since it takes nearly a year to synthesize and fully characterize a new electro-optic material, theoretical simulations are extremely important for quickly identifying structures that will advance the state-of-the-art by minimizing trial and error (Edisonian) development of chromophores. Of course, knowledge of organic chemistry must be utilized in selecting chromophore structures to be examined by multiscale simulation methods keeping in mind that it is the product $\rho_N\langle\cos^3\theta\rangle$ that must be optimized. Given that chemical functionalities that can produce cross-linking of chromophores must also be considered to achieve hardened materials (e.g., materials with glass transition temperatures of >170 °C subsequent to poling),[109] it is important to consider modifications that serve multiple purposes. For example, coumarins may be introduced to control the dimensionality of the environment surrounding electro-optic materials and to facilitate cross-linking. Control of viscoelastic properties is also important, and introduction of fluorinated moieties has been shown to be a useful avenue to achieving desired properties. For example, arene-perfluoroarene moieties can be used to influence matrix dimensionality and viscoelastic properties.[109] With all modifications, the price to be paid with respect to lower number density must be considered.

In addition to chromophore modification, mixing two different chromophore systems to create a binary chromophore composite material has been shown to be capable of leading to improved electro-optic activity.[66,100,109] Options include making one of these systems photoactive, e.g., capable of undergoing light-induced changes in molecular conformation. For such a binary chromophore composite, polarized laser radiation can be used to create a material matrix of lower dimensionality and thus enhanced electric field poling efficiency.[109] Such a process is referred to as laser-assisted electric field poling (LAP). If dimensionality is reduced to 2D, a factor of 2 improvement in poling efficiency is predicted and observed experimentally, holding other parameters constant. LAP does suffer from two potential problems:[109] (1) photoinduced conductivity, which makes realization of large electric poling fields difficult, and (2) photoinduced decomposition at very high photon flux. LAP experiments have been carried out in thin films and simple devices and can lead to competitive electro-optic activity. However, such experiments can be difficult to implement for nanoscopic device architectures.

Poling using pyroelectric crystals has also been demonstrated and has shown some success in reducing conductance effects, thus permitting higher electric fields to be used.[112,113] Such poling is particularly useful for preparing thick electro-optic films relevant to THz sensing applications. Conductance is a major problem with poling of OEO materials. Introduction of charge blocking layers has been effectively used to reduce conductance effects and improve poling efficiency in thin film bulk materials.[109,110,113−115] Unfortunately, utilization of charge blocking layers cannot always be easily implemented in nanoscopic devices, but this is an active area of research.

Comparison of the results of simulations using the conventional NVT or NPT ensembles and then with the results when combined with AVA can provide insight into problems of trapping of chromophores in nonequilibrium distributions (local minima), which is particularly a problem for neat chromophore materials. Variation of results for different trajectories in the simulation can likewise provide insight into experimentally observed scatter for different poling experiments. For example, chromophores YLD-124 and JRD-1 are different only with respect to the substituents R^1 and R^2 (see Figure 3);[109] yet, YLD-124 is much more prone to being trapped in local minima with smaller acentric order and thus reduced electro-optic activity. Consideration of the dynamics of poling as well as molecular hyperpolarizability and intermolecular interactions that influence order at true equilibrium is important. Again, functionalities used for cross-linking can also be designed to promote favorable poling kinetics. Substituents that play more than one role are important for achieving desired acentric order without paying an unacceptable price with respect to reducing number density.

Multiscale theoretical simulations have elucidated the complexities of chromophore design and materials processing. Insight has been obtained with respect to the role of specific intermolecular interactions on material dimensionality and poling-induced acentric order. Insight is provided into the dependence of electro-optic activity on slot width and into conductance effects on maximum usable poling field strengths.[109,114] Specific modifications must be considered from the perspective of achieving multiple outcomes, e.g., improving acentric order without paying an excessive price in terms of number density, controlling lattice dimensionality and viscoelasticity, controlling conductance, and achieving a hardened lattice subsequent to electric field poling.

DOI: 10.1021/acsphotonics.7b00224
ACS Photonics 2017, 4, 1576−1590

EVOLUTION OF DEVICE ARCHITECTURES

To illustrate the evolution of device footprint, we focus on device architectures incorporating OEO materials progressing from centimeter scale all-organic devices to silicon−organic hybrid devices featuring lengths of hundreds of micrometers to plasmonic−organic hybrid devices with lengths of less than 100 μm. Lithium niobate devices are commonly much longer, extending to lengths on the order of 10 cm. It is important to realize that device architecture in addition to electro-optic materials will play a critical role in defining performance parameters such as the π-voltage−length product ($U_\pi L$, i.e., the product of the voltage U_π required to achieve a phase shift of π and the length L of the device). Concentration of electromagnetic fields in nanoscopic waveguides will dramatically reduce the $U_\pi L$ product by increasing electric field intensities and by enhancing modal overlap of high-frequency optical fields and lower frequency (dc to THz) radio frequency fields. With plasmonic structures, the group velocity of plasmon polaritons is reduced relative to optical photons so that the interaction time with the modulating electric field is increased. This is referred to as the "slow-light" effect. Since device architecture influences not only performance but also processing (fabrication) options, we attempt to provide an introduction in the following paragraphs to basic architectures incorporating OEO materials.

All-Organic Thin Film Devices.[109] All-organic thin film OEO devices consist of a bottom cladding layer, a core OEO material layer, and a top cladding layer, all sandwiched between top and bottom electrodes (typically gold or indium tin oxide). The index of refraction of the OEO core is higher than that of the cladding materials, so that light is confined primarily in the core by total internal reflection. However, the index contrast between core and cladding materials is modest, requiring relatively thick cladding layers, leading to electrode separation on the order of or greater than 7 μm. The relative conductivity of core and cladding layers is a consideration in predicting the poling field at the core chromophores. Ideally, the cladding materials would have lower optical loss and higher conductivity than the core materials, which is seldom the case[109] For telecommunication wavelengths (centered around 1.3 or 1.55 μm), core thicknesses of 1−2 μm are typical. Electrode separations of greater than 7 μm make achievement of $U_\pi L$ values significantly less than 1 Vcm difficult with current OEO materials. To achieve sub-1 V operation, devices of 1−2 cm in length are typically required, leading to the requirement that OEO core waveguide propagation losses must be less than 2 dB/cm to achieve total insertion loss of less than 5−6 dB. Also, the operational bandwidth of devices is defined not by the active OEO material but by the resistor−capacitor (RC) limit of the device structure. Therefore, short (~1 cm) devices are required for bandwidths approaching 100 GHz. Until 2006, all-organic devices dominated research involving OEO materials for both stripline and resonant device architectures.[109] While all-organic devices offered significant drive voltage and bandwidth performance improvements relative to lithium niobate devices, they still suffered from an unacceptably large footprint for chip-scale integration of electronics and photonics. Given the importance of size, weight, and power, particularly for airborne and space applications, there is a strong motivation to consider device architectures leading to smaller footprints. The relative size of all-organic, SOH, and POH devices is schematically illustrated in Figure 5.[80]

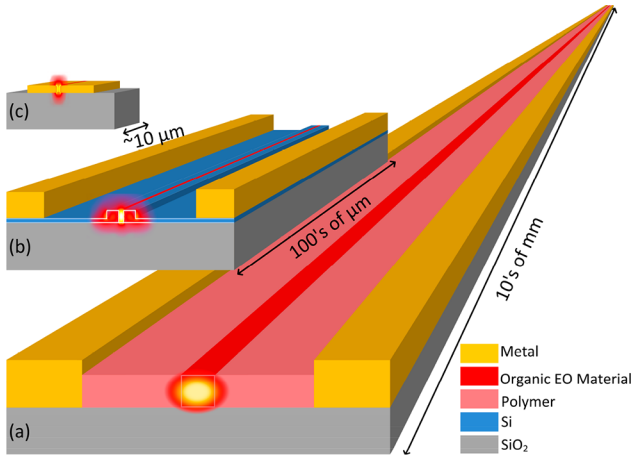

Figure 5. Conceptual representation of various organic modulator architectures (not to scale). (a) All-organic waveguide modulator. Light (optical mode profile) is guided within a waveguide formed by the organic electro-optic material; the phase is modulated by the drive voltage applied across the metal electrodes that drops off over the transverse distance of a few micrometers. Such organic modulator devices have centimeter lengths. (b) Silicon−organic hybrid modulators. The electrical field drops only across the slot filled with the OEO material; this allows strong overlap of optical and RF electric fields, reducing device length to a few hundred micrometers. (c) Plasmonic−organic hybrid modulators exploit stronger confinement of light by surface plasmon polaritons, thereby reducing device lengths to a few tens of micrometers.

Conductance is a well-known problem with all-organic devices, and to reduce such effects, charge-blocking layers are often introduced between the electrodes and the OEO material.[103−105,109−115] Such layers can lead to a doubling of the maximum achievable electro-optic coefficients, e.g., permit realization of activities greater than 500 pm/V.[103−105,109−111]

Thermal and photochemical stability has been a concern for OEO materials, but if the materials are hardened by intermolecular cross-linking reactions subsequent to electric field poling, good thermal and photochemical stability can be achieved.[109] Devices that satisfy Telcordia standards have been demonstrated.[109,116] For the materials discussed here, cross-linking reactions such as Diels−Alder reactions have been shown to elevate the material glass transition temperature, T_g, to 170 °C or greater. It has been shown in many kinetic studies[109] of thermally induced relaxation of poling-induced acentric order that the rate of relaxation can be related to the difference between the measurement temperature and T_g. Long-term thermal stability can be achieved for operating temperatures that are less than 40 °C or more below the material glass transition temperature.[108]

Studies of all-organic devices have illustrated the importance of device architecture on the electro-optic activity that can be achieved by electric field poling of OEO materials.[109] A variety of poling configurations including parallel plate, coplanar electrode, corona, and laser-assisted poling have been investigated.[109] Conductance can be attenuated by introduction of charge-blocking layers.

Silicon−Organic Hybrid Devices.[46−61,63−70,73,76,77,79,81,87,109,117] The high refractive index contrast of Si and SiO_2 permits a reduction in waveguide dimensions to typical widths of 400−500 nm for light of near-IR telecommunication wavelengths. Cutting slots in silicon waveguides allows confinement of light and concentration of

DOI: 10.1021/acsphotonics.7b00224
ACS Photonics 2017, 4, 1576−1590

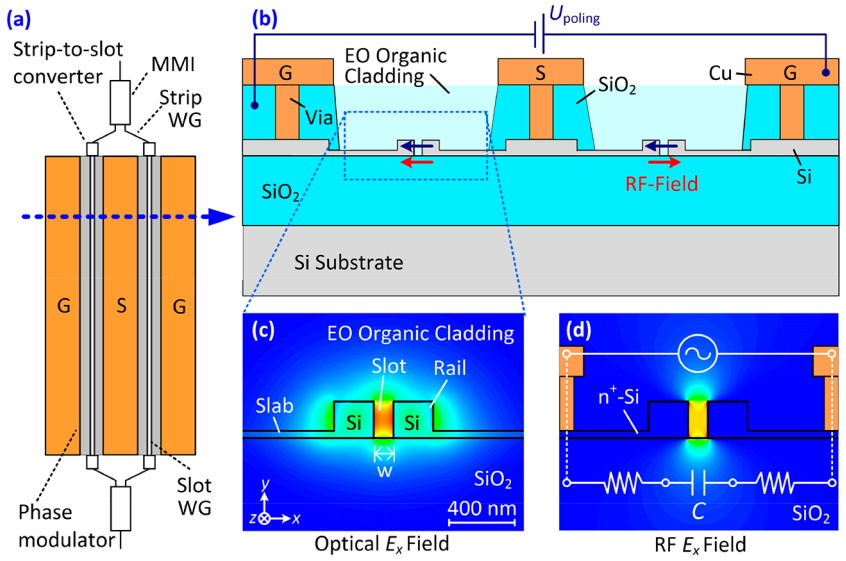

Figure 6. Silicon–organic hybrid (SOH) Mach–Zehnder modulator (MZM). (a) Schematic of the MZM. The device consists of two slot-waveguide (WG) phase modulators, driven in push–pull operation by a single coplanar ground–signal–ground (GSG) transmission line. Before and after the modulator sections, the light is split and combined by multimode interference (MMI) couplers. (b) Cross-section of an SOH MZM using metal vias to connect the GSG transmission line to the Si slot waveguide. Push–pull operation is obtained by an appropriate choice of poling directions (blue arrows) of the EO cladding in both arms with respect to the direction of the local RF field (red arrows). (c) Cross-sectional view and simulated distribution of the dominant electrical component (E_x) of the optical quasi-TE mode field for a single phase modulator (slot width 160 nm, rail width 210 nm, waveguide height 220 nm). The optical mode is strongly confined to the slot due to electric field discontinuities at the slot sidewalls. (d) Simulated E_x component of the RF mode field of the slot waveguide. The modulation voltage drops across the narrow slot, resulting in a high modulation field that has a strong overlap with the optical mode. Adapted with permission from ref 46.

electrical fields in the subwavelength slots filled with lower refractive index materials. When these slots are filled with organic electro-optic materials, the devices are referred to as SOH devices. A schematic illustration of an SOH Mach–Zehnder modulator (MZM) is given in Figure 6a.[46] The SOH phase shifters of the MZM are driven in push–pull mode in a ground–signal–ground configuration. Note that the electric field poling (blue arrows) and radio frequency (RF) drive (red arrows) operations are illustrated in this figure. Each of the phase modulators consists of a slot waveguide, which is filled and covered by the OEO material as shown in the vertical cross-section of an SOH modulator depicted in Figure 6b. The optical mode is strongly confined to the slot region, shown in Figure 6c. The rails of the phase modulators are connected to the metal strips of the transmission line by thin, doped silicon slabs to confine the voltage applied to the transmission line across the narrow slot. This architecture results in a strong modulating RF field that overlaps nearly perfectly with the optical mode; see Figure 6d.

Both vertical (e.g., Figure 6) and horizontal slot waveguides have been demonstrated, and slot widths ranging from 25 nm to greater than 150 nm have been investigated.[109] The tight confinement and strong overlap of optical and radio frequency modes permit a dramatic enhancement of the nonlinear effect. Drive voltages of ≤0.5 V have been realized for modulators with lengths as short as 1 mm, and sub-millimeter devices with bandwidths over 100 GHz have been demonstrated.[64,66,70,76] Low drive voltages (low $U_\pi L$ products) lead to femtojoule/bit energy efficiency and in some cases to even sub-femtojoule/bit (attojoule/bit) efficiency.[66,70] Microring resonators[55,109] and slow-light structures[41−44,51] have been implemented in order to address limitations of millimeter dimensions imposed by transmission (strip) line (e.g., conventional Mach–Zehnder) SOH devices. Moreover microring structures permit signal enhancement (through the Q factor of the ring) and facilitate operations such as wavelength division multiplexing. However, the reduced footprint and signal enhancement come at a high price: The use of resonant structures inherently limits the device bandwidth (through the Q factor) and therefore the suitability for high-speed data transmission applications. Also, ring microring resonators suffer from bending loss, which ultimately places a size limitation on device dimensions.[109]

The short length of SOH devices greatly relaxes the demands on optical propagation loss associated with OEO materials. Optical losses associated with OEO materials will make an insignificant contribution to overall device insertion loss. Short device length also is important for bandwidth, as the properties of drive electrodes will typically define bandwidth for all-organic and SOH devices.

Plasmonic–Organic Hybrid Devices.[46,62,71,72,74,75,78,80,82,83,85,88,89,118−122] Plasmonics is another way to highly confine light in low-refractive-index materials. By exciting surface plasmon polaritons (SPPs), the coupling of photons and charge density oscillations on a metal surface, plasmonics allows light confinement below the diffraction limit as well as strong electric field enhancement. When an organic nonlinear optical material is applied to the metal surface, the nonlinear effects in this material can be efficiently utilized and is often addressed as the plasmonic–organic hybrid technology. Various plasmonic OEO devices have been investigated including both metal–insulator–metal and insulator–metal–insulator architectures. Plasmonic devices have the advantage of facilitating both dramatic reduction in waveguide dimensions (see Figures 5) and permitting high bandwidth operation. Typical concentration of optical and electrical (RF) fields in a POH device structure is shown in Figure 7. Another factor contributing to the enhancement of "effective" optical nonlinearity is the reduced energy velocity of

DOI: 10.1021/acsphotonics.7b00224
ACS Photonics 2017, 4, 1576−1590

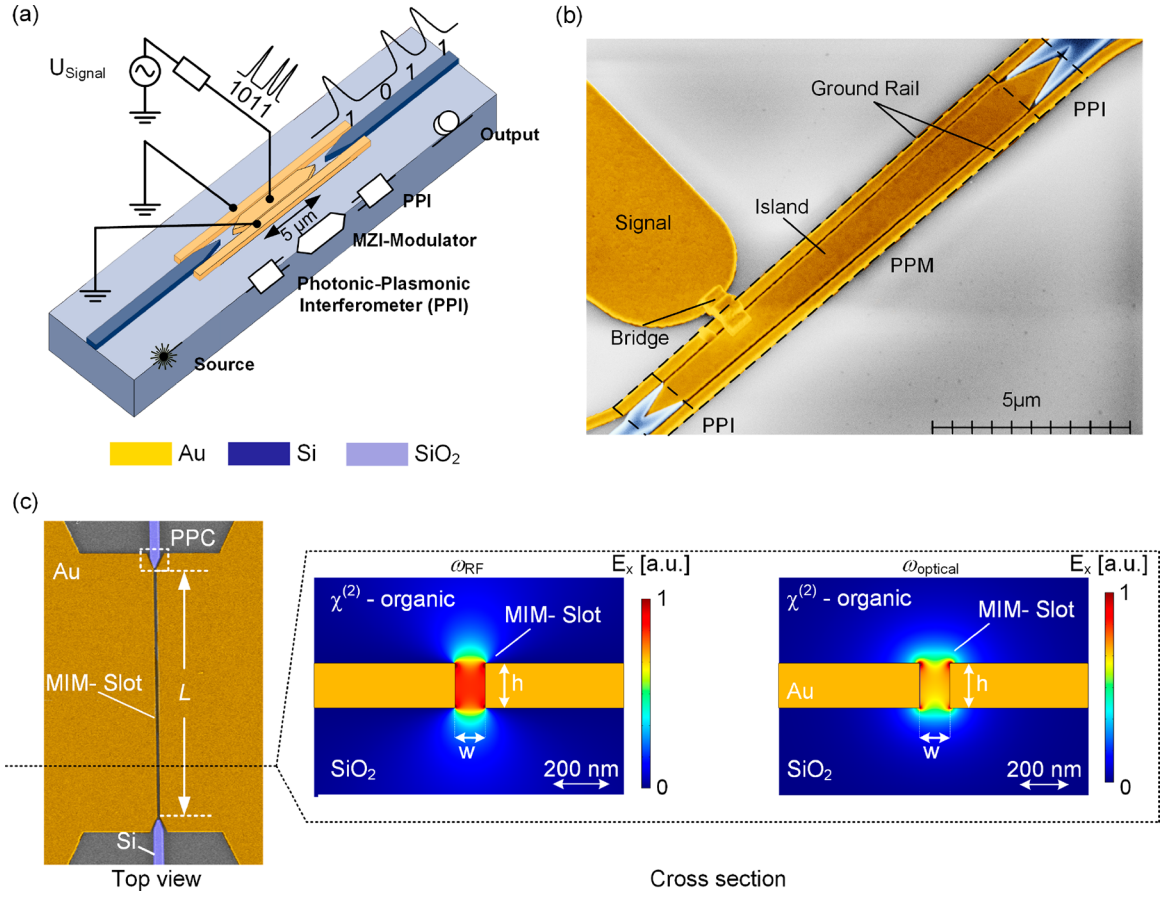

Figure 7. (a) Schematic of a plasmonic−organic hybrid MZM modulator; (b) colorized SEM of such a plasmonic modulator. Efficient photon to plasmon polariton conversion is critical and is achieved with the PPI interferometric devices shown in these figures. (c) Top view and cross-section of a plasmonic phase modulator. The RF and optical mode profiles are overlaid with the cross-section view, highlighting the almost perfect overlap of both fields. Adapted with permission from ref 80.

SPPs. The low (femtosecond) RC time constants of plasmonic structures readily permit bandwidths of several hundred GHz to be achieved.

The challenge of plasmonic structures (as with metamaterial and photonic crystal architectures) is that of optical loss. This concern inhibited exploration of this technology for a number of years, but as with silicon photonics, progress has been made in reducing passive waveguide optical loss. With plasmonic devices, it is unnecessary to utilize resonant structures such as ring resonators or etalons to achieve small dimensions or low drive voltages. The slow-light effect of SPPs, together with the nanoscopic concentration and overlap of fields, leads to dramatic enhancement of nonlinear optical effects making long path lengths unnecessary. Of course, the high optical loss of plasmonic waveguides means that the length of these active waveguides must be kept to a few micrometers and high material electro-optic activity is also crucial to minimizing device length. Efficient conversion from plasmonic waveguides to low loss photonic waveguides is important. A photonic−plasmonic converter (PPC) structure[118−121] for efficient conversion between photons and SPPs is shown in Figure 7c. In this PPC section the feeding silicon waveguide is tapered from a width of typically 450 nm down to zero within a length of approximately 1 μm. The silicon taper ends in the plasmonic slot waveguide, exciting the plasmonic gap mode of the waveguide.

To this point, it has been shown how nanoscopic design of both OEO materials and device architecture has permitted significant reduction in $U_\pi L$. If poling-induced electro-optic activity, r_{33}, did not depend upon waveguide slot width, $U_\pi L$ would continue to decrease with decreasing slot width. However, the poling-induced electro-optic activities (r_{33}) of organic chromophore materials depend upon slot width, reflecting the importance of interactions at interfaces.[86] The dependence on slot width is observed for both composite and monolithic materials, but the electro-optic activity of monolithic materials significantly exceeds that of composite materials.[86] Coarse-grained Monte Carlo simulations also suggest a dependence of r_{33} on slot width, as shown in Figure 4; chromophores tend to lie down with their long axis along the electrode interface (i.e., perpendicular to the normal to the interface: the poling direction).[86] This leads to significant reduction in the effective electro-optic activity. Several factors, including mirror charges, contribute to this phenomenon. Of course, there are other reasons why narrow slots may lead to a reduction in electro-optic activity, including incomplete filling of slots and nonvertical walls.[86] The effect of nonvertical walls has been calculated.[86]

If undesired effects associated with interfaces can be ameliorated, then $U_\pi L$ can be dramatically improved. This may be possible by use of subnanoscopic interfacial layers between electrodes and the OEO material and/or by use of covalent coupling of chromophores and the interface (e.g.,

DOI: 10.1021/acsphotonics.7b00224
ACS Photonics 2017, 4, 1576−1590

sequential synthesis).[109] Theoretical guidance will likely be required to optimize these approaches, as a large number of interactions determine the acentric order that can be realized by various options.

Very recently, the slot width dependence has been further investigated as a function of optical wavelength, adding further insight into the studies just discussed.[122] The optical wavelength dependence provides insight into the role of chromophore absorption related optical loss that comes into play as visible wavelengths are approached. These studies illustrate that improvement in $U_\pi L$ and r_{33} can be achieved by operating at wavelengths shorter than 1.3 μm (but still significantly removed from the λ_{max} of absorptions) using existing chromophores. Alternatively, chromophores with longer π-electron bridges can be utilized to achieve improved $U_\pi L$ and r_{33} values without paying a penalty in optical loss. Such chromophores have been theoretically investigated and recently synthesized and almost certainly will shortly define the state-of-the-art for hybrid OEO-materials-related technologies.

DEVICE AND SYSTEM PERFORMANCE EVALUATION[5,7,14,24,50,56,57,61,62,64,72,80,123−144]

Overview of the Performance of Different Modulation Technologies. Electro-optic devices can be broadly divided into two categories: (1, phase modulation based on the Pockels effect) approaches that produce modulation through mainly a change in the real component of the material's refractive index for a given wavelength and (2, phase and amplitude modulation) approaches that produce modulation through simultaneous change in both the real and imaginary component of the material's refractive index. The latter class suffers from signal "chirp", which limits signal linearity.[143] Examples of this latter class include electroabsorptive modulators, modulators based on the quantum-confined Stark effect in III−V semiconductors,[123−126] modulators based on the Franz−Keldysh effect in silicon−germanium (SiGe),[127−129] and modulators based on free-carrier dispersion effects in silicon (Si).[5−9,14,15,130−135] Another difference among various types of modulation is that of response time to time-varying electric fields. Very fast modulation is possible using organic electro-optic materials, because the femtosecond response to time-varying electrical fields is defined by the phase relaxation of the conjugated π-electron system; this permits potential bandwidths of tens of terahertz, as demonstrated in THz generation and detection, all-optical modulation, pulsed time-resolved experiments,[109] and the frequency dependence of electro-optic experiments.[122] Materials involving electronic excitation can result in device bandwidths being limited by excited-state lifetimes. Currently reported bandwidth and size characteristics of various technologies are shown in Figure 8.[5,7,14,24,56,61,62,64,72,80,85,123−129,133,134,138]

The bandwidth of devices utilizing Pockels effect materials is seldom limited by fundamental characteristics of materials, e.g., phase relaxation of π-electron OEO materials or velocity mismatch of RF and optical waves in the case of lithium niobate. In general, bandwidth of SOH devices is limited by the RC time constant of the slot waveguide structure due to the resistivity of silicon slabs connecting the silicon rails to metal electrodes, shown in Figure 6d. This limitation can be overcome by applying a gate voltage between the substrate and the top silicon layer, which increases the conductivity of the slabs by inducing a charge accumulation layer.[46,141] Plasmonic−organic hybrid devices avoid this limitation, accounting for the bandwidths over 100 GHz easily achieved with such devices.

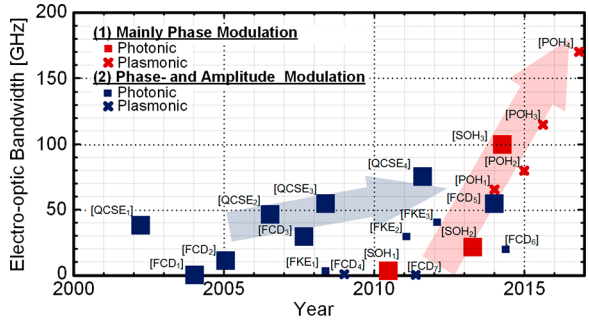

Figure 8. Experimental results for bandwidth and footprint of various integrated electro-optic modulators. The graph shows the improvement of bandwidth over the last 17 years for integrated photonic and plasmonic modulators. The size of the symbol indicates the relative footprint, the color of the symbol indicates the modulation type that it relies on, and the cross and solid square correspond to plasmonic and photonic modulators, respectively. Modulation is based on the following effects: the quantum-confined Stark effect ($QCSE_{1-4}$);[123−126] the Franz−Keldysh effect (FKE_{1-3});[127−129] free carrier dispersion (FCD_{1-7});[5,7,14,24,133,134,138] and the Pockels effect in silicon−organic hybrid (SOH_{1-3})[56,61,64] and plasmonic−organic hybrid (POH_{1-4}).[62,72,80,85] Adapted with permission from ref 80.

POH and SOH modulators reduce the $U_\pi L$ figure-of-merit by more than an order of magnitude in comparison to conventional pn-depletion-type devices on the silicon photonic platform (see Table 1[46]). In this context, another important figure-of-merit results from the fact that the device length is related to the insertion loss via the propagation loss a in the phase shifter section. The quantity a is usually expressed in dB/mm. For pn-depletion-type phase shifters, propagation losses are mainly caused by doping and typically amount to approximately 1 dB/mm, whereas for SOH devices, an upper boundary of 2 dB/mm is estimated for the propagation loss.[46] Plasmonic slot waveguides have considerably higher losses, on the order of 400 dB/mm for current devices based on Au structure, which might be reduced to 200 dB/mm by replacing Au with Ag.[80,132] At the same time, POH devices are significantly shorter than their SOH or depletion-type counterparts, which strongly mitigates the loss issue. Another figure-of-merit relates the product of propagation loss a and the $U_\pi L$ figure-of-merit; see the fourth column in Table 1.[46] The resulting π-voltage−length-loss product has the unit dB V; it corresponds to the product of the phase-shifter insertion loss and the π-voltage and can be interpreted as the π-voltage of a device having a 1 dB insertion loss or, equivalently, as the insertion loss of a device having a π-voltage of 1 V. SOH devices feature the lowest π-voltage−length-loss product, $aU_\pi L \approx 1$ dB V, whereas the corresponding numbers for both depletion-type and POH devices are considerably higher. Interestingly, due to their small $U_\pi L$ product, POH modulators

Table 1. Comparison of Figures-of-Merit of Different Silicon−Photonic and Silicon−Plasmonic Modulator Types[46]

modulator type	$U_\pi L$ [V mm]	a [dB/mm]	$aU_\pi L$ [dB V]
pn-depletion	10.00	001	10
SOH	0.50	002	01
POH	0.05	200	10

DOI: 10.1021/acsphotonics.7b00224
ACS Photonics 2017, 4, 1576−1590

show similar performance to depletion-type modulators regarding the π-voltage−length-loss product. Of course, improving OEO activity (r_{33}) will reduce $U_\pi L$ and $aU_\pi L$, leading to further improvement of the figures-of-merit for the SOH and POH devices.

The high signal purity (linearity, as in spur-free dynamic range or bit error ratio) enabled by Pockels effect modulators accounts for the popularity of lithium niobate modulators, which have been used for all of the important telecommunication systems demonstrations to date.[17] However, the large size of lithium niobate modulators (5−10 cm) makes this technology impractical for chip-scale integration of electronics and photonics. A large Pockels effect together with the fastest response available with OEO materials and the ability to use large-scale silicon photonic or plasmonic integration provides the fundamental motivation for pursuing SOH and POH devices. Cost, ease of integration with diverse materials, and potential for improvement in electro-optic activity, optical transparency, and stability (thermal and photochemical) provide the additional motivations.

Silicon photonics, plasmonics, and photonic crystal architectures provide routes to (subwavelength) miniaturization of photonic circuitry and to the concentration of optical and electrical fields for enhanced performance. Plasmonics and photonic crystal architectures also afford the opportunity to exploit the "slow-light effect". Taken together, the integration of organic electro-optic materials with new device architectures (creating a hybrid technology) provides an attractive route to chip-scale integration of electronics and photonics and accounts for the many orders of magnitude improvement in performance, which was recently demonstrated. Various figures-of-merit (FOMs) have been defined to compare various technologies. A common FOM is the product of $U_\pi L$ and optical loss. SOH devices currently afford the best performance for this FOM (see Table 1). For some applications, very high bandwidth may also be important, as will other factors such as long-term stability under accelerated aging conditions.

It is important to keep in mind that SOH and POH device performance is rapidly evolving, driven through advances in OEO materials and device architectures. For example, within the past several months in-device electro-optic activity has been increased from 230 pm/V[66] to >350 pm/V.[87] As noted above, further development of new neat chromophore materials is underway and will likely lead to another doubling of in-device electro-optic activity (with corresponding reduction of $U_\pi L$ and $aU_\pi L$) in the coming year. It should be kept in mind that in addition to theoretically suggested improvements in molecular first hyperpolarizability, it is very reasonable that acentric order can be further improved. The current best obtainable values of $\langle \cos^3 \theta \rangle$ are on the order of 0.2. Theory suggests that poling-induced order can be improved by as much as a factor of 2 by further modification of chromophore shape. Improvement may also be possible through implementation of charge-blocking layers and by exploitation of "designed" covalent and noncovalent interactions, with the maximum possible improvement being a factor of 5. Of course, for every modification, the impact on chromophore number density must be considered, and theory has already demonstrated that optimizing acentric order typically comes at the price of some reduction in number density. Nevertheless, the combination of improvements in molecular hyperpolarizability together with optimization of the product of number density and acentric order should lead to a factor of 3−4 improvement of in-device electro-optic activity. This value is below the ultimate theoretical limit.[140]

Performance in Telecommunication Systems. Phase modulators are the building blocks of Mach−Zehnder modulators. In turn, MZMs are the critical building blocks of in-phase-quadrature (IQ) modulators commonly used in telecommunication applications.[83] The effective bandwidth of telecommunication systems has been enhanced by wavelength division multiplexing, which has benefitted from use of ring microresonator devices and comb sources[68] that provide the closely spaced carrier wavelengths necessary for increasing bandwidth by "color coding" information. Advanced modulation formats are extremely important for the coding and high-throughput transmission of digital information in telecommunication applications. Common formats include binary phase shift keying, bipolar amplitude shift keying, quadrature phase shift keying (QPSK), m-state quadrature amplitude modulation (QAM), etc.

SOH and POH MZMs have been shown to be viable for high-speed data transmission at the lowest power consumption.[46,85] In a scheme where data are encoded into two intensity levels of the optical signal (on−off keying), a data rate of 100 Gbit/s has been demonstrated.[77,85] To increase the data rate, more information can be encoded into the optical signal by using multiple intensity levels. In a four-level pulse amplitude modulation (PAM-4)[85,141] scheme, SOH and POH modulators have been used to generate signals at 120 Gbit/s. Alternatively, complex modulation formats encode data in both the phase and the magnitude of the optical field (IQ modulation). Using two nested SOH MZMs in an IQ-modulator configuration, data rates of 252 Gbit/s have been demonstrated using a 16QAM scheme.[83] By combining two POH MZMs with an IQ configuration, modulators generating advanced modulation formats (QPSK, 16QAM) on a footprint of only 10 μm × 75 μm became possible.[80] The high modulation efficiency of organic-hybrid modulators can greatly simplify the electronic drive circuitry.[142] It is possible to directly drive the modulators with the binary outputs of state-of-the-art CMOS circuits.[76] The generation of QAM signals using subvoltage SOH modulators, without any digital-to-analog converters or amplifiers, has been shown.[76] High-speed operation of SOH modulators at elevated temperature has been demonstrated for symbol rates of up to 64 GBd.[81]

Diverse Device Architectures and Applications. Two major areas of electro-optic technology include optical interconnects and RF (microwave) photonics. The former involves digital signal processing, while the latter involves analog signal processing. The bit error ratio (BER) defines the signal quality for the former, while spur-free dynamic range (SFDR) defines signal linearity for the latter. SOH and POH devices have exhibited competitive BER and SFDR values, although performance has yet to be fully optimized for these hybrid devices.

Telecommunication applications have been discussed in the preceding paragraphs. Microwave photonics is illustrated by detection of microwaves employing a plasmonic antenna[78,98,144] and in beam steering applications.[84] Such antenna architectures permit signal enhancement of nearly 100 000. This is an example of radio frequency field detection reflecting that fields from dc to THz can be detected. Indeed, a wide variety of chemical and physical phenomena can be sensed utilizing electro-optics.[109] The small dimensions of plasmonic architectures can be exploited for single-molecule detection. A

DOI: 10.1021/acsphotonics.7b00224
ACS Photonics 2017, 4, 1576−1590

variety of architectures can be combined to implement the transmitter and receiver sections of phased array radar. Devices ranging from ultrasound detectors to optical gyroscopes can be implemented.[109]

CONCLUSIONS

Significant progress has been made relevant to chip-scale integration of electronics and photonics through multiscale theory guided improvement of organic electro-optic materials and through exploitation of novel plasmonic and silicon photonic device architectures. Important improvements of device performance have been achieved, including with respect to $U_\pi L$ (drive voltage and footprint), bandwidth, energy efficiency, and insertion loss. Multiscale theory has permitted a quantitative understanding of the dependence of electric field poling induced electro-optic activity upon chromophore shape and upon introduced dipolar and quadrupolar interactions that influence longer range chromophore cooperativity (lattice dimensionality). Chromophore modification is shown to influence both poling-induced acentric order and chromophore number density, and the trade-off between these two contributions to macroscopic electro-optic activity must be carefully considered for each putative modification. Theory also suggests that molecular hyperpolarizability can be further improved through modification of the chromophore core and that the accompanying improvement in electro-optic activity can be realized without a noticeable impact on device insertion loss (particularly for POH devices where plasmonic losses dominate propagation loss[122]). It is important to use chromophore organization (molecular ensembles) defined by coarse-grained statistical mechanical calculations in quantum mechanical calculations of linear and nonlinear optical properties to appropriately account for excitonic effects. SOH and POH device performance has also been improved through the concentration of optical and radio frequency fields in nanoslot waveguides and for POH devices through the "slow-light" effect. Simulation of chromophore poling induced order has also been carried out for chromophores in nanoslot waveguides as a function of slot width.[86] These calculations illustrate the organization of chromophores at interfaces and suggest how electro-optic activity can be improved for nanoslot waveguides with dimensions of 20−80 nm (by modification of chromophore and electrode structures). Simulation results for narrow slots also suggest that self-assembly/sequential synthesis methods[109] may be used to improve acentric order, although theory-guided design of chromophore structures and covalent coupling motifs will be important for the optimization of the product of chromophore acentric order and number density. Thus, theory suggests that device performance can be substantially improved in the future. Realization of in-device electro-optic activity of >1000 pm/V and $U_\pi L$ values of <10 Vμm are not unreasonable near-term objectives for future research.

AUTHOR INFORMATION

Corresponding Author

*E-mail: dalton@chem.washington.edu.

ORCID

Wolfgang Heni: 0000-0003-0861-2530
Lewis E. Johnson: 0000-0002-7412-073X
Delwin L. Elder: 0000-0001-9302-3858
Bruce H. Robinson: 0000-0002-5579-953X
Larry R. Dalton: 0000-0002-6461-0145

Author Contributions

[⊥]W. Heni and Y. Kutuvantavida contributed equally to the published work.

Notes

The authors declare no competing financial interest.

ACKNOWLEDGMENTS

The authors acknowledge the National Science Foundation (DMR-1303080), the Air Force Office of Scientific Research (FA9550-15-1-0319), the European Research Council (ERC Starting Grant "EnTeraPIC", number 280145), the European Research Council PLASILOR project (EU-670478), the EU-FP7 projects PHOXTROT and BigPipes, and the Helmholtz International Research School for Teratronics (HIRST). The research of C. Koos was supported by the Alfried Krupp Prize for Young University Teachers of the Krupp Foundation. L.R.D. acknowledges the receipt of a Helmholtz International Award for Excellent Researchers and Science Managers from Abroad. Helpful discussions with Professor Alvin Kwiram are also acknowledged.

REFERENCES

(1) Reed, G. T.; Knights, A. P. *Silicon Photonics: An Introduction*. Wiley: West Sussex, England, 2004.
(2) Almeida, V. R.; Xu, Q.; Barrios, C. A.; Lipson, M. Guiding and confining light in void nanostructure. *Opt. Lett.* **2004**, *29*, 1209−1211.
(3) Lockwood, D. J.; Pavesi, L. Silicon fundamentals for photonics applications. In *Silicon Photonics*; Pavesi, L.; Lockwood, D. J., Eds.; Springer-Verlag: Berlin, 2004; Vol. *94*, pp 1−50.
(4) Vlasov, Y. A.; McNab, S. J. Losses in single-mode silicon-on-insulator strip waveguides and bends. *Opt. Express* **2004**, *12*, 1622−1631.
(5) Liu, A. S.; Jones, R.; Liao, L.; Samara-Rubio, D.; Rubin, D.; Cohen, O.; Nicolaescu, R.; Paniccia, M. A high-speed silicon optical modulator based on a metal-oxide-semiconductor capacitor. *Nature* **2004**, *427*, 615−618.
(6) Lipson, M. Guiding, modulating, and emitting light on silicon - Challenges and opportunities. *J. Lightwave Technol.* **2005**, *23*, 4222−4238.
(7) Liao, L.; Samara-Rubio, D.; Morse, M.; Liu, A. S.; Hodge, D.; Rubin, D.; Keil, U. D.; Franck, T. High speed silicon Mach-Zehnder modulator. *Opt. Express* **2005**, *13*, 3129−3135.
(8) Gardes, F. Y.; Reed, G. T.; Emerson, N. G.; Png, C. E. A sub-micron depletion-type photonic modulator in Silicon On Insulator. *Opt. Express* **2005**, *13*, 8845−8854.
(9) Xu, Q. F.; Schmidt, B.; Pradhan, S.; Lipson, M. Micrometre-scale silicon electro-optic modulator. *Nature* **2005**, *435*, 325−327.
(10) Jalali, B.; Fathpour, S. Silicon photonics. *J. Lightwave Technol.* **2006**, *24*, 4600−4615.
(11) Xu, Q. F.; Schmidt, B.; Shakya, J.; Lipson, M. Cascaded silicon micro-ring modulators for WDM optical interconnection. *Opt. Express* **2006**, *14*, 9430−9435.
(12) Gunn, C. CMOS photonics for high-speed interconnects. *IEEE Micro* **2006**, *26*, 58−66.
(13) Soref, R. The past, present, and future of silicon photonics. *IEEE J. Sel. Top. Quantum Electron.* **2006**, *12*, 1678−1687.
(14) Liu, A. S.; Liao, L.; Rubin, D.; Nguyen, H.; Ciftcioglu, B.; Chetrit, Y.; Izhaky, N.; Paniccia, M. High-speed optical modulation based on carrier depletion in a silicon waveguide. *Opt. Express* **2007**, *15*, 660−668.
(15) Liao, L.; Liu, A.; Rubin, D.; Basak, J.; Chetrit, Y.; Nguyen, H.; Cohen, R.; Izhaky, N.; Paniccia, M. 40 Gbit/s silicon optical modulator for high-speed applications. *Electron. Lett.* **2009**, 51−52.
(16) Reed, G. T.; Mashanovich, G.; Gardes, F. Y.; Thomson, D. J. Silicon optical modulators. *Nat. Photonics* **2010**, *4*, 518−526.

DOI: 10.1021/acsphotonics.7b00224
ACS Photonics 2017, 4, 1576−1590

(17) Chen, A.; Murphy, E. J. *Broadband Optical Modulators: Science, Technology, and Applications*; CRC Press: Boca Raton, FL, 2012.
(18) Dong, P.; Chen, Y. K.; Duan, G. H.; Neilson, D. T. Silicon photonic devices and integrated circuits. *Nanophotonics* **2014**, *3*, 215−228.
(19) Luo, L. W.; Ophir, N.; Chen, C. P.; Gabrielli, L. H.; Poitras, C. B.; Bergmen, K.; Lipson, M. WDM-compatible mode-division multiplexing on a silicon chip. *Nat. Commun.* **2014**, *5*, 7.
(20) Subbaraman, H.; Xu, X. C.; Hosseini, A.; Zhang, X. Y.; Zhang, Y.; Kwong, D.; Chen, R. T. Recent advances in silicon-based passive and active optical interconnects. *Opt. Express* **2015**, *23*, 2487−2510.
(21) Bowers, J. E.; Komljenovic, T.; Davenport, M.; Hulme, J.; Liu, A. Y.; Santis, C. T.; Spott, A.; Srinivasan, S.; Stanton, E. J.; Zhang, C. Recent advances in silicon photonic integrated circuits. *Proc. SPIE* **2016**, *9774*, 977402−977402−18.
(22) Thomson, D.; Zilkie, A.; Bowers, J. E.; Komljenovic, T.; Reed, G. T.; Vivien, L.; Marris-Morini, D.; Cassan, E.; Virot, L.; Fedeli, J. M.; Hartmann, J. M.; Schmid, J. H.; Xu, D. X.; Boeuf, F.; O'Brien, P.; Mashanovich, G. Z.; Nedeljkovic, M. Roadmap on silicon photonics. *J. Opt.* **2016**, *18*, 073003.
(23) Ozbay, E. Plasmonics: Merging photonics and electronics at nanoscale dimensions. *Science* **2006**, *311*, 189−193.
(24) Dionne, J. A.; Diest, K.; Sweatlock, L. A.; Atwater, H. A. PlasMOStor: A metal-oxide-Si field effect plasmonic modulator. *Nano Lett.* **2009**, *9*, 897−902.
(25) Gramotnev, D. K.; Bozhevolnyi, S. I. Plasmonics beyond the diffraction limit. *Nat. Photonics* **2010**, *4*, 83−91.
(26) Sorger, V. J.; Oulton, R. F.; Ma, R. M.; Zhang, X. Toward integrated plasmonic circuits. *MRS Bull.* **2012**, *37*, 728−738.
(27) Kriesch, A.; Burgos, S. P.; Ploss, D.; Pfeifer, H.; Atwater, H. A.; Peschel, U. Functional plasmonic nanocircuits with low insertion and propagation losses. *Nano Lett.* **2013**, *13*, 4539−4545.
(28) Lee, H. W.; Papadakis, G.; Burgos, S. P.; Chander, K.; Kriesch, A.; Pala, R.; Peschel, U.; Atwater, H. A. Nanoscale conducting oxide PlasMOStor. *Nano Lett.* **2014**, *14*, 6463−6468.
(29) Fang, Y. R.; Sun, M. T. Nanoplasmonic waveguides: towards applications in integrated nanophotonic circuits. *Light: Sci. Appl.* **2015**, *4*, 11.
(30) Krasavin, A. V.; Zayats, A. V. Active nanophotonic circuitry based on dielectric-loaded plasmonic waveguides. *Adv. Opt. Mater.* **2015**, *3*, 1662−1690.
(31) Kinsey, N.; Ferrera, M.; Shalaev, V. M.; Boltasseva, A. Examining nanophotonics for integrated hybrid systems: a review of plasmonic interconnects and modulators using traditional and alternative materials Invited. *J. Opt. Soc. Am. B* **2015**, *32*, 121−142.
(32) Soljacic, M.; Johnson, S. G.; Fan, S. H.; Ibanescu, M.; Ippen, E.; Joannopoulos, J. D. Photonic-crystal slow-light enhancement of nonlinear phase sensitivity. *J. Opt. Soc. Am. B* **2002**, *19*, 2052−2059.
(33) Vlasov, Y. A.; O'Boyle, M.; Hamann, H. F.; McNab, S. J. Active control of slow light on a chip with photonic crystal waveguides. *Nature* **2005**, *438*, 65−69.
(34) Krauss, T. F. Slow light in photonic crystal waveguides. *J. Phys. D: Appl. Phys.* **2007**, *40*, 2666−2670.
(35) Wulbern, J. H.; Petrov, A.; Eich, M. Electro-optical modulator in a polymer-infiltrated silicon slotted photonic crystal waveguide heterostructure resonator. *Opt. Express* **2009**, *17*, 304−313.
(36) Lin, C. Y.; Wang, X. L.; Chakravarty, S.; Lee, B. S.; Lai, W. C.; Luo, J. D.; Jen, A. K. Y.; Chen, R. T. Electro-optic polymer infiltrated silicon photonic crystal slot waveguide modulator with 23 dB slow light enhancement. *Appl. Phys. Lett.* **2010**, *97*, 3.
(37) Wang, X. L.; Lin, C. Y.; Chakravarty, S.; Luo, J. D.; Jen, A. K. Y.; Chen, R. T. Effective in-device r(33) of 735 pm/V on electro-optic polymer infiltrated silicon photonic crystal slot waveguides. *Opt. Lett.* **2011**, *36*, 882−884.
(38) Notomi, M.; Shinya, A.; Nozaki, K.; Tanabe, T.; Matsuo, S.; Kuramochi, E.; Sato, T.; Taniyama, H.; Sumikura, H. Low-power nanophotonic devices based on photonic crystals towards dense photonic network on chip. *IET Circ. Devices Syst.* **2011**, *5*, 84−93.
(39) Nguyen, H. C.; Sakai, Y.; Shinkawa, M.; Ishikura, N.; Baba, T. Photonic Crystal silicon optical modulators: Carrier-injection and depletion at 10 Gb/s. *IEEE J. Quantum Electron.* **2012**, *48*, 210−220.
(40) Nguyen, H. C.; Hashimoto, S.; Shinkawa, M.; Baba, T. Compact and fast photonic crystal silicon optical modulators. *Opt. Express* **2012**, *20*, 22465−22474.
(41) Zhang, X. Y.; Hosseini, A.; Chakravarty, S.; Luo, J. D.; Jen, A. K. Y.; Chen, R. T. Wide optical spectrum range, subvolt, compact modulator based on an electro-optic polymer refilled silicon slot photonic crystal waveguide. *Opt. Lett.* **2013**, *38*, 4931−4934.
(42) Inoue, S.; Otomo, A. Electro-optic polymer/silicon hybrid slow light modulator based on one-dimensional photonic crystal waveguides. *Appl. Phys. Lett.* **2013**, *103*, 4.
(43) Zhang, X. Y.; Hosseini, A.; Subbaraman, H.; Wang, S. Y.; Zhan, Q. W.; Luo, J. D.; Jen, A. K. Y.; Chen, R. T. Integrated photonic electromagnetic field sensor based on broadband bowtie antenna coupled silicon organic hybrid modulator. *J. Lightwave Technol.* **2014**, *32*, 3774−3784.
(44) Zhang, X. Y.; Chung, C. J.; Hosseini, A.; Subbaraman, H.; Luo, J. D.; Jen, A. K. Y.; Nelson, R. L.; Lee, C. Y. C.; Chen, R. T. High performance optical modulator based on electro-optic polymer filled silicon slot photonic crystal waveguide. *J. Lightwave Technol.* **2016**, *34*, 2941−2951.
(45) Yan, H.; Xu, X.; Chung, C.-J.; Subbaraman, H.; Pan, Z.; Chakravarty, S.; Chen, R. T. One-dimensional photonic crystal slot waveguide for silicon-organic hybrid electro-optic modulators. *Opt. Lett.* **2016**, *41*, 5466−5469.
(46) Koos, C.; Leuthold, J.; Freude, W.; Kohl, M.; Dalton, L.; Bogaerts, W.; Giesecke, A. L.; Lauermann, M.; Melikyan, A.; Koeber, S.; Wolf, S.; Weimann, C.; Muehlbrandt, S.; Koehnle, K.; Pfeifle, J.; Hartmann, W.; Kutuvantavida, Y.; Ummethala, S.; Palmer, R.; Korn, D.; Alloatti, L.; Schindler, P. C.; Elder, D. L.; Wahlbrink, T.; Bolten, J. Silicon-organic hybrid (SOH) and plasmonic-organic hybrid (POH) integration. *J. Lightwave Technol.* **2016**, *34*, 256−268.
(47) Baehr-Jones, T.; Hochberg, M.; Wang, G. X.; Lawson, R.; Liao, Y.; Sullivan, P. A.; Dalton, L.; Jen, A. K. Y.; Scherer, A. Optical modulation and detection in slotted Silicon waveguides. *Opt. Express* **2005**, *13*, 5216−5226.
(48) Hochberg, M.; Baehr-Jones, T.; Wang, G. X.; Shearn, M.; Harvard, K.; Luo, J. D.; Chen, B. Q.; Shi, Z. W.; Lawson, R.; Sullivan, P.; Jen, A. K. Y.; Dalton, L.; Scherer, A. Terahertz all-optical modulation in a silicon-polymer hybrid system. *Nat. Mater.* **2006**, *5*, 703−709.
(49) Hochberg, M.; Baehr-Jones, T.; Wang, G.; Huang, J.; Sullivan, P.; Dalton, L.; Scherer, A. Towards a millivolt optical modulator with nano-slot waveguides. *Opt. Express* **2007**, *15*, 8401−8410.
(50) Baehr-Jones, T.; Penkov, B.; Huang, J. Q.; Sullivan, P.; Davies, J.; Takayesu, J.; Luo, J. D.; Kim, T. D.; Dalton, L.; Jen, A.; Hochberg, M.; Scherer, A. Nonlinear polymer-clad silicon slot waveguide modulator with a half wave voltage of 0.25 V. *Appl. Phys. Lett.* **2008**, *92*, 3.
(51) Brosi, J. M.; Koos, C.; Andreani, L. C.; Waldow, M.; Leuthold, J.; Freude, W. High-speed low-voltage electro-optic modulator with a polymer-infiltrated silicon photonic crystal waveguide. *Opt. Express* **2008**, *16*, 4177−4191.
(52) Vallaitis, T.; Bogatscher, S.; Alloatti, L.; Dumon, P.; Baets, R.; Scimeca, M. L.; Biaggio, I.; Diederich, F.; Koos, C.; Freude, W.; Leuthold, J. Optical properties of highly nonlinear silicon-organic hybrid (SOH) waveguide geometries. *Opt. Express* **2009**, *17*, 17357−17368.
(53) Leuthold, J.; Freude, W.; Brosi, J. M.; Baets, R.; Dumon, P.; Biaggio, I.; Scimeca, M. L.; Diederich, F.; Frank, B.; Koos, C. Silicon organic hybrid technology-A platform for practical nonlinear optics. *Proc. IEEE* **2009**, *97*, 1304−1316.
(54) Koos, C.; Vorreau, P.; Vallaitis, T.; Dumon, P.; Bogaerts, W.; Baets, R.; Esembeson, B.; Biaggio, I.; Michinobu, T.; Diederich, F.; Freude, W.; Leuthold, J. All-optical high-speed signal processing with silicon-organic hybrid slot waveguides. *Nat. Photonics* **2009**, *3*, 216−219.

DOI: 10.1021/acsphotonics.7b00224
ACS Photonics 2017, 4, 1576−1590

(55) Takayesu, J.; Hochberg, M.; Baehr-Jones, T.; Chan, E.; Wang, G. X.; Sullivan, P.; Liao, Y.; Davies, J.; Dalton, L.; Scherer, A.; Krug, W. A hybrid electrooptic microring resonator-based 1 × 4 x 1 ROADM for wafer scale optical interconnects. *J. Lightwave Technol.* **2009**, *27*, 440−448.
(56) Ding, R.; Baehr-Jones, T.; Liu, Y.; Bojko, R.; Witzens, J.; Huang, S.; Luo, J.; Benight, S.; Sullivan, P.; Fedeli, J. M.; Fournier, M.; Dalton, L.; Jen, A.; Hochberg, M. Demonstration of a low $V_{\pi}L$ modulator with GHz bandwidth based on electro-optic polymer-clad silicon slot waveguides. *Opt. Express* **2010**, *18*, 15618−15623.
(57) Gould, M.; Baehr-Jones, T.; Ding, R.; Huang, S.; Luo, J. D.; Jen, A. K. Y.; Fedeli, J. M.; Fournier, M.; Hochberg, M. Silicon-polymer hybrid slot waveguide ring-resonator modulator. *Opt. Express* **2011**, *19*, 3952−3961.
(58) Alloatti, L.; Korn, D.; Weimann, C.; Koos, C.; Freude, W.; Leuthold, J. Second-order nonlinear silicon-organic hybrid waveguides. *Opt. Express* **2012**, *20*, 20506−20515.
(59) Palmer, R.; Alloatti, L.; Korn, D.; Schindler, P. C.; Baier, M.; Bolten, J.; Wahlbrink, T.; Waldow, M.; Dinu, R.; Freude, W.; Koos, C.; Leuthold, J. Low power Mach-Zehnder modulator in silicon-organic hybrid technology. *IEEE Photonics Technol. Lett.* **2013**, *25*, 1226−1229.
(60) Leuthold, J.; Koos, C.; Freude, W.; Alloatti, L.; Palmer, R.; Korn, D.; Pfeifle, J.; Lauermann, M.; Dinu, R.; Wehrli, S.; Jazbinsek, M.; Gunter, P.; Waldow, M.; Wahlbrink, T.; Bolten, J.; Kurz, H.; Fournier, M.; Fedeli, J. M.; Yu, H.; Bogaerts, W. Silicon-organic hybrid electro-optical devices. *IEEE J. Sel. Top. Quantum Electron.* **2013**, *19*, 114−126.
(61) Korn, D.; Palmer, R.; Yu, H.; Schindler, P. C.; Alloatti, L.; Baier, M.; Schmogrow, R.; Bogaerts, W.; Selvaraja, S. K.; Lepage, G.; Pantouvaki, M.; Wouters, J. M. D.; Verheyen, P.; Van Campenhout, J.; Chen, B. Q.; Baets, R.; Absil, P.; Dinu, R.; Koos, C.; Freude, W.; Leuthold, J. Silicon-organic hybrid (SOH) IQ modulator using the linear electro-optic effect for transmitting 16QAM at 112 Gbit/s. *Opt. Express* **2013**, *21*, 13219−13227.
(62) Melikyan, A.; Alloatti, L.; Muslija, A.; Hillerkuss, D.; Schindler, P. C.; Li, J.; Palmer, R.; Korn, D.; Muehlbrandt, S.; Van Thourhout, D.; Chen, B.; Dinu, R.; Sommer, M.; Koos, C.; Kohl, M.; Freude, W.; Leuthold, J. High-speed plasmonic phase modulators. *Nat. Photonics* **2014**, *8*, 229−233.
(63) Palmer, R.; Alloatti, L.; Korn, D.; Schindler, P. C.; Schmogrow, R.; Heni, W.; Koenig, S.; Bolten, J.; Wahlbrink, T.; Waldow, M.; Yu, H.; Bogaerts, W.; Verheyen, P.; Lepage, G.; Pantouvaki, M.; Van Campenhout, J.; Absil, P.; Dinu, R.; Freude, W.; Koos, C.; Leuthold, J. Silicon-organic hybrid MZI modulator generating OOK, BPSK and 8-ASK signals for up to 84 Gbit/s. *IEEE Photonics J.* **2013**, *5*, 7.
(64) Alloatti, L.; Palmer, R.; Diebold, S.; Pahl, K. P.; Chen, B. Q.; Dinu, R.; Fournier, M.; Fedeli, J. M.; Zwick, T.; Freude, W.; Koos, C.; Leuthold, J. 100 GHz silicon-organic hybrid modulator. *Light: Sci. Appl.* **2014**, *3*, e173.
(65) Korn, D.; Jazbinsek, M.; Palmer, R.; Baier, M.; Alloatti, L.; Yu, H.; Bogaerts, W.; Lepage, G.; Verheyen, P.; Absil, P.; Guenter, P.; Koos, C.; Freude, W.; Leuthold, J. Electro-optic organic crystal silicon high-speed modulator. *IEEE Photonics J.* **2014**, *6*, 9.
(66) Palmer, R.; Koeber, S.; Elder, D. L.; Woessner, M.; Heni, W.; Korn, D.; Lauermann, M.; Bogaerts, W.; Dalton, L.; Freude, W.; Leuthold, J.; Koos, C. High-speed, low drive-voltage silicon-organic hybrid modulator based on a binary-chromophore electro-optic material. *J. Lightwave Technol.* **2014**, *32*, 2726−2734.
(67) Lauermann, M.; Palmer, R.; Koeber, S.; Schindler, P. C.; Korn, D.; Wahlbrink, T.; Bolten, J.; Waldow, M.; Elder, D. L.; Dalton, L. R.; Leuthold, J.; Freude, W.; Koos, C. Low-power silicon-organic hybrid (SOH) modulators for advanced modulation formats. *Opt. Express* **2014**, *22*, 29927−29936.
(68) Weimann, C.; Schindler, P. C.; Palmer, R.; Wolf, S.; Bekele, D.; Korn, D.; Pfeifle, J.; Koeber, S.; Schmogrow, R.; Alloatti, L.; Elder, D.; Yu, H.; Bogaerts, W.; Dalton, L. R.; Freude, W.; Leuthold, J.; Koos, C. Silicon-organic hybrid (SOH) frequency comb sources for terabit/s data transmission. *Opt. Express* **2014**, *22*, 3629−3637.
(69) Lauermann, M.; Wolf, S.; Palmer, R.; Koeber, S.; Schindler, P. C.; Wahlbrink, T.; Bolten, J.; Giesecke, A. L.; Koenigsmann, M.; Kohler, M.; Malsam, D.; Elder, D. L.; Dalton, L. R.; Leuthold, J.; Freude, W.; Koos, C. High-speed and low-power silicon-organic hybrid modulators for advanced modulation formats. *Proc. SPIE* **2016**, *951607*, 951607−951607−5.
(70) Koeber, S.; Palmer, R.; Lauermann, M.; Heni, W.; Elder, D. L.; Korn, D.; Woessner, M.; Alloatti, L.; Koenig, S.; Schindler, P. C.; Yu, H.; Bogaerts, W.; Dalton, L. R.; Freude, W.; Leuthold, J.; Koos, C. Femtojoule electro-optic modulation using a silicon-organic hybrid device. *Light: Sci. Appl.* **2015**, *4*, 8.
(71) Heni, W.; Hoessbacher, C.; Haffner, C.; Fedoryshyn, Y.; Baeuerle, B.; Josten, A.; Hillerkuss, D.; Salamin, Y.; Bonjour, R.; Melikyan, A.; Kohl, M.; Elder, D. L.; Dalton, L. R.; Hafner, C.; Leuthold, J. High speed plasmonic modulator array enabling dense optical interconnect solutions. *Opt. Express* **2015**, *23*, 29746−29757.
(72) Haffner, C.; Heni, W.; Fedoryshyn, Y.; Niegemann, J.; Melikyan, A.; Elder, D. L.; Baeuerle, B.; Salamin, Y.; Josten, A.; Koch, U.; Hoessbacher, C.; Ducry, F.; Juchli, L.; Emboras, A.; Hillerkuss, D.; Kohl, M.; Dalton, L. R.; Hafner, C.; Leuthold, J. All-plasmonic Mach-Zehnder modulator enabling optical high-speed communication at the microscale. *Nat. Photonics* **2015**, *9*, 525−528.
(73) Lauermann, M.; Wolf, S.; Schindler, P. C.; Palmer, R.; Koeber, S.; Korn, D.; Alloatti, L.; Wahlbrink, T.; Bolten, J.; Waldow, M.; Koenigsmann, M.; Kohler, M.; Malsam, D.; Elder, D. L.; Johnston, P. V.; Phillips-Sylvain, N.; Sullivan, P. A.; Dalton, L. R.; Leuthold, J.; Freude, W.; Koos, C. 40 GBd 16QAM signaling at 160 Gb/s in a silicon-organic hybrid modulator. *J. Lightwave Technol.* **2015**, *33*, 1210−1216.
(74) Melikyan, A.; Koehnle, K.; Lauermann, M.; Palmer, R.; Koeber, S.; Muehlbrandt, S.; Schindler, P. C.; Elder, D. L.; Wolf, S.; Heni, W.; Haffner, C.; Fedoryshyn, Y.; Hillerkuss, D.; Sommer, M.; Dalton, L. R.; Van Thourhout, D.; Freude, W.; Kohl, M.; Leuthold, J.; Koos, C. Plasmonic-organic hybrid (POH) modulators for OOK and BPSK signaling at 40 Gbit/s. *Opt. Express* **2015**, *23*, 9938−9946.
(75) Heni, W.; Haffner, C.; Baeuerle, B.; Fedoryshyn, Y.; Josten, A.; Hillerkuss, D.; Niegemann, J.; Melikyan, A.; Kohl, M.; Elder, D. L.; Dalton, L. R.; Hafner, C.; Leuthold, J. 108 Gbit/s plasmonic Mach-Zehnder modulator with > 70-GHz electrical bandwidth. *J. Lightwave Technol.* **2016**, *34*, 393−400.
(76) Wolf, S.; Lauermann, M.; Schindler, P.; Ronniger, G.; Geistert, K.; Palmer, R.; Kober, S.; Bogaerts, W.; Leuthold, J.; Freude, W.; Koos, C. DAC-less amplifier-less generation and transmission of QAM signals using sub-volt silicon-organic hybrid modulators. *J. Lightwave Technol.* **2015**, *33*, 1425−1432.
(77) Hartmann, W.; Lauermann, M.; Wolf, S.; Zwickel, H.; Kutuvantavida, Y.; Luo, J.; Jen, A. K.-Y.; Freude, W.; Koos, C. 100 Gbit/s OOK using a silicon-organic hybrid (SOH) modulator. 41th European Conf. Opt. Commun. (ECOC'15), Valencia, Spain, Sept. 27−Oct. 5, 2015, Paper PDP1.4.
(78) Salamin, Y.; Heni, W.; Haffner, C.; Fedoryshyn, Y.; Hoessbacher, C.; Bonjour, R.; Zahner, M.; Hillerkuss, D.; Leuchtmann, P.; Elder, D. L.; Dalton, L. R.; Hafner, C.; Leuthold, J. Direct conversion of free space millimeter waves to optical domain by plasmonic modulator antenna. *Nano Lett.* **2015**, *15*, 8342−8346.
(79) Lauermann, M.; Weimann, C.; Knopf, A.; Heni, W.; Palmer, R.; Koeber, S.; Elder, D. L.; Bogaerts, W.; Leuthold, J.; Dalton, L. R.; Rembe, C.; Freude, W.; Koos, C. Integrated optical frequency shifter in silicon-organic hybrid (SOH) technology. *Opt. Express* **2016**, *24*, 1694−1707.
(80) Haffner, C.; Heni, W.; Fedoryshyn, Y.; Josten, A.; Baeuerle, B.; Hoessbacher, C.; Salamin, Y.; Koch, U.; Dordevic, N.; Mousel, P.; Bonjour, R.; Emboras, A.; Hillerkuss, D.; Leuchtmann, P.; Elder, D. L.; Dalton, L.; Hafner, C.; Leuthold, J. Plasmonic organic hybrid modulators-scaling highest speed photonics to the microscale. *Proc. IEEE* **2016**, *104*, 2362−2379.
(81) Lauermann, M.; Wolf, S.; Hartmann, W.; Palmer, R.; Kutuvantavida, Y.; Zwickel, H.; Bielik, A.; Altenhain, L.; Lutz, J.; Schmid, R.; Wahlbrink, T.; Bolten, J.; Giesecke, A. L.; Freude, W.; Koos, C. Generation of 64 GBd 4ASK signals using a silicon-organic hybrid modulator at 80 degrees C. *Opt. Express* **2016**, *24*, 9389−9396.

DOI: 10.1021/acsphotonics.7b00224
ACS Photonics 2017, 4, 1576−1590

(82) Hoessbacher, C.; Salamin, Y.; Fedoryshyn, Y.; Heni, W.; Josten, A.; Baeuerle, B.; Haffner, C.; Zahner, M.; Chen, H.; Elder, D. L.; Wehrli, S.; Hillerkuss, D.; Van Thourhout, D.; Van Campenhout, J.; Dalton, L. R.; Hafner, C.; Leuthold, J. Optical interconnect with densely integrated plasmonic modulator and germanium photodetector Arrays. Optical Fiber Communication Conference, Anaheim, California March 20−22, 2016, Paper Th1F.6.
(83) Wolf, S.; Lauermann, M.; Hartmann, W.; Zwickel, H.; Kutuvantavida, Y.; Koenigsmann, M.; Gruen, M.; Luo, J.; Jen, A. K.; Freude, W.; Koos, C. An energy-efficient 252 Gbit/s silicon-based IQ-modulator. Optical Fiber Communication Conference, Anaheim, California March 20−22, 2016, Paper Th3J.2.
(84) Bonjour, R.; Burla, M.; Abrecht, F. C.; Welschen, S.; Hoessbacher, C.; Heni, W.; Gebrewold, S. A.; Baeuerle, B.; Josten, A.; Salamin, Y.; Haffner, C.; Johnston, P. V.; Elder, D. L.; Leuchmann, P.; Hillerkuss, D.; Fedoryshyn, Y.; Dalton, L. R.; Hafner, C.; Leuthold, J. Plasmonic phased array feeder enabling ultra-fast beam steering at millimeter waves. *Opt. Express* **2016**, *24*, 25608−25618.
(85) Hoessbacher, C.; Josten, A.; Baeuerle, B.; Fedoryshyn, Y.; Hettrich, H.; Salamin, Y.; Heni, W.; Haffner, C.; Schmid, R.; Elder, D. L.; Hillerkuss, D.; Moller, M.; Dalton, L. R.; Leuthold, J. Plasmonic modulator with > 170 GHz bandwidth demonstrated at 100 Gbit/s NRZ. *Opt. Express* **2017**, *25*, 1762−1768.
(86) Heni, W.; Haffner, C.; Elder, D. L.; Fedoryshyn, Y.; Cottier, R.; Salamin, Y.; Hoessbacher, C.; Tillack, A. F.; Robinson, B.; Hafner, C.; Dalton, L. R.; Leuthold, J. Nonlinearities of organic electro-optic materials in nanoscale slots and the implications for the optimum modulator design. *Opt. Express* **2017**, *25*, 2627−2653.
(87) Kieninger, C.; Kutuvantavida, Y.; Zwickel, H.; Wolf, S.; Lauermann, M.; Elder, D.; Dalton, L. R.; Freude, W.; Randel, S.; Koos, C. Record-high in-device electro-optic coefficient of 359 pm/V in a silicon-organic hybrid modulator. Conference on Lasers and Electro-Optics, San Jose Convention Center, CA, USA, May 14−17, 2017.
(88) Hoessbacher, C.; Josten, A.; Baeuerle, B.; Fedoryshyn, Y.; Hettrich, H.; Salamin, Y.; Heni, W.; Haffner, C.; Schmid, R.; Elder, D. L.; Hillerkuss, D.; M?ller, M.; Dalton, L. R.; Leuthold, M. *Broadband plasmonic modulator enabling single carrier operation beyond 100 Gbit/s.* Optical Networking and Communication Conference (OFC 2017), Los Angles, CA, USA, March 19−23, 2017.
(89) Burla, M.; Bonjour, R.; Salamin, Y.; Haffner, C.; Heni, W.; Hosessbacher, C.; Fedoryshyn, Y.; Abrecht, F. C.; Johnston, P. V.; Elder, D. L.; Dalton, L. R.; Leuthold, J. Microwave plasmonics: A novel platform for RF photonics. Proceedings MWP/AVFOP 2016, Avionics and Vehicle Fiber-Optics and Photonics Conference and IEEE International Topical Meeting on Microwave Photonics (MWP), October 31−November 3, 2016, Long Beach, CA, pp 259−262.
(90) Roelkens, G.; Liu, L.; Liang, D.; Jones, R.; Fang, A.; Koch, B.; Bowers, J. III-V/silicon photonics for on-chip and inter-chip optical interconnects. *Laser Photon. Rev.* **2010**, *4*, 751−779.
(91) Cheung, S.; Kawakita, Y.; Shang, K. P.; Ben Yoo, S. J. Highly efficient chip-scale III-V/silicon hybrid optical amplifiers. *Opt. Express* **2015**, *23*, 22431−22443.
(92) Zhang, C.; Morton, P. A.; Khurgin, J. B.; Peters, J. D.; Bowers, J. E. Highly linear heterogeneous-integrated Mach-Zehnder interferometer modulators on Si. *Opt. Express* **2016**, *24*, 19040−19047.
(93) Sun, Z.; Martinex, A.; Wang, F. Opritcal modulators with 2D layered materials. *Nat. Photonics* **2016**, *10*, 227−238.
(94) Wooten, E. L.; Kissa, K. M.; Yi-Yan, A.; Murphy, E. J.; Lafaw, D. A.; Hallemeier, P. F.; Maack, D.; Attanasio, D. V.; Fritz, D. J.; McBrien, G. J.; Bossi, D. E. A review of lithium niobate modulators for fiber-optic communications systems. *IEEE J. Sel. Top. Quantum Electron.* **2000**, *6*, 69−82.
(95) Korn, D.; Lauermann, M.; Koeber, S.; Appel, P.; Alloatti, L.; Palmer, R.; Dumon, P.; Freude, W.; Leuthold, J.; Koos, C. Lasing in silicon-organic hybrid waveguides. *Nat. Commun.* **2016**, *7*, 9.
(96) Dalton, L. R.; Harper, A. W.; Robinson, B. H. The role of London forces in defining noncentrosymmetric order of high dipole moment high hyperpolarizability chromophores in electrically poled polymeric thin films. *Proc. Natl. Acad. Sci. U. S. A.* **1997**, *94*, 4842−4847.
(97) Robinson, B. H.; Dalton, L. R. Monte Carlo statistical mechanical simulations of the competition of intermolecular electrostatic and poling-field interactions in defining macroscopic electro-optic activity for organic chromophore/polymer materials. *J. Phys. Chem. A* **2000**, *104*, 4785−4795.
(98) Shi, Y. Q.; Zhang, C.; Zhang, H.; Bechtel, J. H.; Dalton, L. R.; Robinson, B. H.; Steier, W. H. Low (sub-1-V) halfwave voltage polymeric electro-optic modulators achieved by controlling chromophore shape. *Science* **2000**, *288*, 119−122.
(99) Dalton, L. R.; Robinson, B. H.; Jen, A. K. Y.; Steier, W. H.; Nielsen, R. Systematic development of high bandwidth, low drive voltage organic electro-optic devices and their applications. *Opt. Mater.* **2003**, *21*, 19−28.
(100) Pereverzev, Y. V.; Gunnerson, K. N.; Prezhdo, O. V.; Sullivan, P. A.; Liao, Y.; Olbricht, B. C.; Akelaitis, A. J. P.; Jen, A. K. Y.; Dalton, L. R. Guest-host cooperativity in organic materials greatly enhances the nonlinear optical response. *J. Phys. Chem. C* **2008**, *112*, 4355−4363.
(101) Dalton, L. R.; Sullivan, P. A.; Bale, D. H. Electric field poled organic electro-optic materials: State of the art and future prospects. *Chem. Rev.* **2010**, *110*, 25−55.
(102) Dalton, L. R.; Benight, S. J.; Johnson, L. E.; Knorr, D. B.; Kosilkin, I.; Eichinger, B. E.; Robinson, B. H.; Jen, A. K. Y.; Overney, R. M. Systematic nanoengineering of soft matter organic electro-optic materials. *Chem. Mater.* **2011**, *23*, 430−445.
(103) Johnson, L. E. v. d. L. Multi-Scale Modeling of Organic Electro-Optic Materials. Ph.D. Thesis, University of Washington, Seattle, WA, USA, 2012.
(104) Tillack, A. F.; Johnson, L. E.; Rawal, M.; Dalton, L. R.; Robinson, B. H. Modeling chromophore order: A guide for improving EO performance. *MRS Online Proc. Libr.*; 2014; 1698, mrss14-1698-jj08-05, *1698*10.1557/opl.2014.795.
(105) Johnson, L. E.; Dalton, L. R.; Robinson, B. H. Optimizing calculations of electronic excitations and relative hyperpolarizabilities of electrooptic chromophores. *Acc. Chem. Res.* **2014**, *47*, 3258−3265.
(106) Robinson, B. H.; Johnson, L. E.; Eichinger, B. E. Relation of system dimensionality and order parameters. *J. Phys. Chem. B* **2015**, *119* (7), 3205−3212.
(107) Tillack, A. F. Electro-Optic Material Design Criteria Derived from Condensed Matter Simulations using the Level-of-Detail Coarse-Graining Approach. Ph.D. Thesis, University of Washington, Seattle, WA, USA, 2015.
(108) Tillack, A. F.; Robinson, B. H. Toward optimal EO response from ONLO chromophores: a statistical mechanics study of optimizing shape. *J. Opt. Soc. Am. B* **2016**, *33*, E121−E129.
(109) Dalton, L. R.; Günter, P.; Jazbinsek, M.; Kwon, O.-P.; Sullivan, P. A. *Organic Electro-Optics and Photonics: Molecules, Polymers, and Crystals*; Cambridge University Press: Cambridge, UK, 2015.
(110) Jin, W. W.; Johnston, P. V.; Elder, D. L.; Tillack, A. F.; Olbricht, B. C.; Song, J. S.; Reid, P. J.; Xu, R. M.; Robinson, B. H.; Dalton, L. R. Benzocyclobutene barrier layer for suppressing conductance in nonlinear optical devices during electric field poling. *Appl. Phys. Lett.* **2014**, *104*, 5.
(111) Elder, D. L.; Benight, S. J.; Song, J. S.; Robinson, B. H.; Dalton, L. R. Matrix-assisted poling of monolithic bridge-disubstituted organic NLO chromophores. *Chem. Mater.* **2014**, *26*, 872−874.
(112) Huang, S.; Luo, J.; Yip, H.-L.; Ayazi, A.; Zhou, X.-H.; Gould, M.; Chen, A.; Baehr-Jones, M.; Hochberg, M.; Jen, A. K.-Y. Efficient poling of electro-optic polymers in thin films and silicon slot waveguides by detachable pyroelectric crystals. *Adv. Mater.* **2012**, *24*, OP42−7.
(113) Enami, Y.; Yuan, B.; Tanaka, M.; Luo, J.; Jen, A. K.-Y. Electro-optic polymer/TiO2 multilayer slot waveguide modulators. *Appl. Phys. Lett.* **2012**, *101*, 123509.
(114) Huang, S.; Luo, J.; Jin, Z.; Li, M.; Kim, T.-D.; Chen, A.; Jen, A. K.-Y. Spontaneously poling of electro-optic polymer thin films across a

DOI: 10.1021/acsphotonics.7b00224
ACS Photonics 2017, 4, 1576−1590

1.1-mm thick glass substrate by pyroelectric crystals. *Appl. Phys. Lett.* **2014**, *105*, 183305.
(115) Enami, Y.; Nakamura, H.; Jen, A. K.-Y. Analysis of efficiently poled electro-optic polymer/TiO2 vertical slot waveguide modulators. *Opt. Commun.* **2016**, *362*, 77−80.
(116) Dinu, R.; Jin, D.; Yu, G. M.; Chen, B. Q.; Huang, D. Y.; Chen, H.; Barklund, A.; Miller, E.; Wei, C. L.; Vemagiri, J. Environmental stress testing of electro-optic polymer modulators. *J. Lightwave Technol.* **2009**, *27*, 1527−1532.
(117) Qiu, F.; Sato, H.; Spring, A. M.; Maeda, D.; Ozawa, M.; Odoi, K.; Aoki, I.; Otomo, A.; Yokoyama, S. Ultra-thin silicon/electro-optic polymer hybrid waveguide modulators. *Appl. Phys. Lett.* **2015**, *107*, 123302.
(118) Veronis, G.; Fan, S. Theoretical investigation of compact couplers between dielectric slab waveguides and two-dimensional metal-dielectric-metal plasmonic waveguides. *Opt. Express* **2007**, *15*, 1211−1221.
(119) Chen, C.-T.; Xu, X.; Hosseini, A.; Pan, Z.; Subbaraman, H.; Zhang, X.; Chen, R. T. Desgin of highly efficient hybrid Si-Au taper for dielectric strip waveguide to plasmonic slot waveguide mode converter. *J. Lightwave Technol.* **2015**, *33*, 535−540.
(120) Tian, J.; Yu, S.; Yan, W.; Qiu, M. Broadband high-efficiency surface-plasmon-polariton coupler with silicon-metal interface. *Appl. Phys. Lett.* **2009**, *95*, 013504.
(121) Ono, M.; Taniyama, H.; Xu, H.; Tsunekawa, M.; Kuramochi, E.; Nozaki, K.; Notomi, M. Deep-subwavelength plasmonic mode converter with large size reduction for Si-wire waveguide. *Optica* **2016**, *3*, 999−1005.
(122) Haffner, C.; Heni, W.; Elder, D. L.; Fedoryshyn, Y.; Dordevic, N.; Chelladurai, D.; Koch, U.; Portner, K.; Burla, M.; Robinson, B.; Dalton, L. R.; Leuthold, J. Harnessing nonlinearities near material absorption resoances for reducing losses in plasmonic modulators. *Opt. Mater. Express* **2017**, *7*, 2168−2181.
(123) Choi, W. J.; Bond, A. E.; Kim, J.; Zhang, R. M.; Jambunathan, R.; Foulk, H.; O'Brien, S.; Van Norman, J.; Vandegrift, D.; Wanamaker, C.; Shakespeare, J.; Cao, H. Low insertion loss and low dispersion penalty InGaAsP quantum-well high-speed electroabsorption modulator for 40-Gb/s very-short-reach, long-reach, and long-haul applications. *J. Lightwave Technol.* **2002**, *20*, 2052−2056.
(124) Fukano, H.; Yamanaka, T.; Tamura, M.; Kondo, Y. Very-low-driving-voltage electroabsorption modulators operating at 40 Gb/s. *J. Lightwave Technol.* **2006**, *24*, 2219−2224.
(125) Wu, T. H.; Chiu, Y. J.; Lin, F. Z. High-speed (60 GHz) and low-voltage-driving electroabsorption modulator using two-consecutive-steps selective-undercut-wet-etching waveguide. *IEEE Photonics Technol. Lett.* **2008**, *20*, 1261−1263.
(126) Tang, Y. B.; Peters, J. D.; Bowers, J. E. Over 67 GHz bandwidth hybrid silicon electroabsorption modulator with asymmetric segmented electrode for 1.3 mu m transmission. *Opt. Express* **2012**, *20*, 11529−11535.
(127) Liu, J.; Beals, M.; Pomerene, A.; Bernardis, S.; Sun, R.; Cheng, J.; Kimerling, L. C.; Michel, J. Waveguide-integrated, ultralow-energy GeSi electro-absorption modulators. *Nat. Photonics* **2008**, *2*, 433−437.
(128) Chaisakul, P.; Marris-Morini, D.; Rouifed, M. S.; Isella, G.; Chrastina, D.; Frigerio, J.; Le Roux, X.; Edmond, S.; Coudevylle, J. R.; Vivien, L. 23 GHz Ge/SiGe multiple quantum well electro-absorption modulator. *Opt. Express* **2012**, *20*, 3219−3224.
(129) Feng, N. N.; Feng, D. Z.; Liao, S. R.; Wang, X.; Dong, P.; Liang, H.; Kung, C. C.; Qian, W.; Fong, J.; Shafiiha, R.; Luo, Y.; Cunningham, J.; Krishnamoorthy, A. V.; Asghari, M. 30 GHz Ge electro-absorption modulator integrated with 3 mm silicon-on-insulator waveguide. *Opt. Express* **2011**, *19*, 7062−7067.
(130) Koos, C.; Brosi, J.; Waldow, M.; Freude, W.; Leuthold, J. Silicon-on-Insulator modulators for next-generation 100 Gbit/s-Ethernet. Optical Communication (ECOC), 2007 33rd European Conference and Exhibition of 2007; pp 1−2.
(131) Dong, P.; Chen, L.; Chen, Y. K. High-speed low-voltage single-drive push-pull silicon Mach-Zehnder modulators. *Opt. Express* **2012**, *20*, 6163−6169.
(132) Dong, P.; Liu, X.; Chandrasekhar, S.; Buhl, L. L.; Aroca, R.; Chen, Y. K. Monolithic silicon photonic integrated circuits for compact 100(+)Gb/s coherent optical receivers and transmitters. *IEEE J. Sel. Top. Quantum Electron.* **2014**, *20*, 8.
(133) Xu, H.; Li, X. Y.; Xiao, X.; Zhou, P. J.; Li, Z. Y.; Yu, J. Z.; Yu, Y. D. High-speed silicon modulator with band equalization. *Opt. Lett.* **2014**, *39*, 4839−4842.
(134) Timurdogan, E.; Sorace-Agaskar, C. M.; Sun, J.; Hosseini, E. S.; Biberman, A.; Watts, M. R. An ultralow power athermal silicon modulator. *Nat. Commun.* **2014**, *5*, 11.
(135) Alloatti, L.; Lauermann, M.; Surgers, C.; Koos, C.; Freude, W.; Leuthold, J. Optical absorption in silicon layers in the presence of charge inversion/accumulation or ion implantation. *Appl. Phys. Lett.* **2013**, *103*, 5.
(136) Rodes, R.; Mueller, M.; Li, B. M.; Estaran, J.; Jensen, J. B.; Gruendl, T.; Ortsiefer, M.; Neumeyr, C.; Rosskopf, J.; Larsen, K. J.; Amann, M. C.; Monroy, I. T. High-Speed 1550 nm VCSEL data transmission link employing 25 GBd 4-PAM modulation and hard decision forward error correction. *J. Lightwave Technol.* **2013**, *31*, 689−695.
(137) Kuchta, D. M.; Doany, F. E.; Schares, L.; Neumeyr, C.; Daly, A.; Kögel, B.; Rosskopf, J.; Ortsiefer, M. Error-free 56 Gb/s NRZ. modulation of a 1530 nm VCSEL link. 41st European Conf. Opt. Commun. (ECOC'15), Valencia, Spain, Sept. 27−Oct. 1, 2015; pp 1−3.10.1109/ECOC.2015.7341677.
(138) Melikyan, A.; Lindenmann, N.; Walheim, S.; Leufke, P. M.; Ulrich, S.; Ye, J.; Vincze, P.; Hahn, H.; Schimmel, T.; Koos, C.; Freude, W.; Leuthold, J. Surface plasmon polariton absorption modulator. *Opt. Express* **2011**, *19*, 8855−8869.
(139) Sorger, V. J.; Lanzillotti-Kimura, N. D.; Ma, R. M.; Zhang, X. Ultra-compact silicon nanophotonic modulator with broadband response. *Nanophotonics* **2012**, *1*, 17−22.
(140) *J. Opt. Soc. Am. B*, special issue, Nonlinear Optics near the Fundamental Limit. December 1, **2016**, *33*, 2414−2655; Feat. pp E1−E181.
(141) Zwickel, H.; Wolf, S.; Kutuvantavida, Y.; Kieninger, C.; Lauermann, M.; Freude, W.; Koos, C. 120 Gbit/s PAM-4 signaling using a silicon-organic hybrid (SOH) Mach-Zehnder modulator. 42th European Conf. Opt. Commun. (ECOC'16), Düsseldorf, Germany, Sept. 18−22, 2016.
(142) Zwickel, H.; De Keulenaer, T.; Wolf, S.; Kieninger, C.; Kutuvantavida, Y.; Lauermann, M.; Verplaetse, M.; Pierco, R.; Vaernewyck, R.; Vyncke, A.; Yin, X.; Torfs, G.; Freude, W.; Mentovich, E.; Bauwelinck, J.; Koos, C. 100 Gbit/s serial transmission using a silicon-organic hybrid (SOH) modulator and a duobinary driver IC. Optical Fiber Communication Conference (OFC'17), Los Angeles (CA), USA, March 19−23, 2017.
(143) Agrawal, G. P. *Lightwave Technology: Components and Devices*; Wiley: New York, NY, USA, 2004.
(144) Zhang, X.; Chung, C.-J.; Subbaraman, H.; Pan, Z.; Chen, C.-T.; Chen, R. T. Design of plasmonic-organic hybrid slot waveguide integrated with a bowtie-antenna for terahertz wave detection. *Proc. SPIE* **2016**, *975614*, 975614−975618.

DOI: 10.1021/acsphotonics.7b00224
ACS Photonics 2017, 4, 1576−1590